Distribution
Category UC-92

SAND840568
Unlimited Release
Printed May 1984

Creep and Creep Modeling of Three Domal Salts-A Comprehensive Update

Wolfgang R. *Wawersik* and David *H.* Zeuch
Geomechanics Division 1542
Sandia National Laboratories
Albuquerque, New Mexico 87185

ABSTRACT

Stress and temperature change tests are described to determine upper and lower bounds of the rates of steady state creep for three domal salts. Results obtained are compared with published data for salt from the same sites and with two larger data sets for a bedded salt. The various data sets are then correlated in activation analyses and fitted by models for power-law creep, cross-slip, and dislocation glide to show that a cross-slip model yields the best and mechanistically most credible fit. This suggestion is consistent with limited substructure observations for one sample. No satisfactory fit was obtained for a two-mechanism model for dislocation climb and cross-slip. Results described include stress drop measurements that demonstrate slow recovery. It remains to be proved if recovery of rock salt at low temperature will be complete, and if so, after how much strain.Although all creep data are described most satisfactorily in terms of cross-slip, power-law models continue to be good empirical approximations. Therefore, the further use of power-law creep equations to describe the steady state creep of rock salt in SPR design calculations is deemed justified.

Contents

Acknowledgments

We owe much gratitude to D. W. Hannum and J. A. Zirzow for their skills, care, and patience in performing many laboratory tests and repeated instrument calibrations. This work could not have been completed without their assistance. We also acknowledge several helpful discussions with G. M. Pharr, W. B. Jones, and W. Skrotzki. Finally, we thank the members of the projects for the Waste Isolation Pilot Plant and the Strategic Petroleum Reserve at Sandia National Laboratories. They allowed us to gather information for a considerable period of time before attempting another synthesis of measurements that proved to be quite difficult because of extremely low creep rates and sample variability.

List of Symbols

L_0, L	undeformed and deformed sample lengths
A_0, A_n	undeformed and deformed sample areas
e_1, e_3	greatest and smallest (most and least compressive) principal strains
γ	shear strain
e	volumetric strain
γ_t, e_{1t}	transient creep strains
$\dot{e}_1, \dot{\gamma}$	strain rates
$\dot{e}_{1b}, \dot{e}_{1e}$	strain rates at beginning and end of creep test
$\dot{e}_{1s}, \dot{\gamma}_s$	steady state creep rates
$\dot{e}_{1u}, \dot{e}_{1l}$	upper and lower bound steady state creep estimates
σ_1, σ_3	greatest and smallest principal (compressive) stresses
$\tau = \sigma_1 - \sigma_3$	shear stress
τ_b	back stress
$\tau_e = \tau - \tau_b$	effective stress
μ	shear modulus
T	temperature in degrees Kelvin for thermodynamic calculations or in degrees Celsius to specify test temperatures
R	universal gas constant
t	time
γ_a, ξ	transient creep parameters
n	power-law stress exponent
Q, Q_{SD}, Q_{SC}	activation energies
$B_1, \cdots, B_8$	creep fitting parameters
V	activation volume
A	activation area

b	Burgers vector
τ_0	flow stress at absolute zero
PO	shear modulus at absolute zero
G, AG	Gibbs free energies
$\Delta H, \Delta H_i, \Delta H_{0i}$	activation enthalpies
S	entropy
C, D_i, D	structure factors
SE	standard error of logarithm of fitted creep equations
a	subgrain size

Stress is given in psi at the request of the SPR project staff at the U.S. Department of Energy and at Sandia National Laboratories. For the same reason, lengths are expressed in feet or inches except in the discussion of substructures.

1 Introduction and Purpose

This report treats extensions of earlier creep measurements on rock salt to support constitutive modeling and finite element calculations used in designing storage caverns for the US Strategic Petroleum Reserve (SPR). The work presented was carried out to meet five practical objectives. (1) Verify that the stress exponent, n, in the steady state creep model for rock salt from West Hackberry is the same as that of bedded salt from the Salado formation, whose response was studied in much greater detail [1-3]. Identical n-values were implied by the agreement between estimates of steady state creep rates for the two salt types. However, this point was never proved because previous tests on West Hackberry core were limited to one stress, τ = 2900 psi. (2) Assure that the creep properties of West Hackberry salt from drillhole SC, tested previously, are representative of samples from other drillholes. (3) Substantiate previous suggestions that rock salt from the Bryan Mound dome creeps much less than do other salt types for which measurements are available [4], such as domal salt from West Hackberry, Avery Island or Asse [5-8], and bedded salt from the Salado formation or from Lyons, Kansas [1,2,9]. (4) Extend the creep data base of the SPR project to include rock salt from Bayou Choctaw, Louisiana, and determine the steady state creep parameters to be used in analyses of Bayou Choctaw caverns. (5) Evaluate the recovery characteristics of rock salt after decreases in stress. This task appeared necessary to test whether creep transients can be neglected under all loading conditions, as is done in current design analyses, because the governing time constant of transient creep is assumed as less than 7 days throughout. To date, transients have been suggested to be short-lived only following stress increases [2,10].

The approach to testing and interpreting previous salt creep data for the SPR relied heavily on recent experience in the characterization of natural rock salt from the Salado formation and from the Asse anticline in the Federal Republic of Germany [7,11,12]. Both sites are being considered for radioactive waste isolation. The conditions of stress and temperature under these projects include the service range of salt surrounding the SPR caverns. Two observations made under the radioactive waste programs were used. First, it was assumed that the total creep of salt, 7, is the sum of transient and steady state creep [1,2],

$$7 = \gamma_t + \dot{\gamma}_s \cdot t. \tag{1}$$

It was further stipulated that transient creep can be described by an exponential function of time [2]

$$\gamma_t = \gamma_a(1 - e^{-\xi t}). \tag{2}$$

Given these expressions it appeared possible to obtain good estimates of the rates of steady state creep from nonlinear least-squares fits of Eqs (1) and (2) to experimental

data [11]. This method was deemed reliable even if relatively short tests ($t \leq 250$ hr) were used where the total creep is dominated by transients and where creep often had not clearly reached steady state.

Second, after the interpretation of Salado and Asse salt data, it was also assumed that steady state creep is described well by a "power-law" of the form

$$\dot{\gamma}_s = C \exp(-Q/RT) \left(\frac{\tau}{\mu}\right)^n \tag{3}$$

where μ is an average shear modulus, and R is the universal gas constant [1,13]. In this study, the shear stress τ denotes the maximum difference in principal stresses $(\sigma_1 - \sigma_3)$. Therefore, τ equals the deviatoric stress under the axisymmetric conditions of triaxial tests. C and Q are constants. Predetermining an applicable creep law greatly facilitated the required test program for SPR. Tests could be carried out at the high end of the stresses of interest where the creep rates were relatively fast $(\approx 10^{-8}\ s^{-1})$ and the maximum test times less than 500 hours. Moreover, it was reasonable to assume that the creep parameters C, Q and n were those of Salado salt, for example, if the steady state creep rate for West Hackberry salt at any stress and temperature was essentially the same as the average steady state creep rate of Salado salt under identical conditions.

Based on additional testing and further analysis of old data, some of the observations of the waste isolation programs proved less certain than they appeared three years ago when creep measurements for West Hackberry and Bryan Mound salt were first published and discussed. Estimates of steady state creep rates often turned out to be high and a function of test duration leading to incorrect values for Q and n [8]. The applicability of power-law creep Eq (3), at low stresses also had to be questioned.

Because of these developments, the work of this report extends beyond addressing the five engineering objectives discussed at the outset. The report also presents some new approaches to determining rates of steady state creep. Finally, it deals with the likely accuracy of the power-law creep model, coupled with some alternate interpretations of the data using new creep measurements for Bryan Mound salt and related results for Salado salt. The evaluation of all creep models is supported by activation analyses and by some, although limited observations of substructures.

2 Material Description

The salt tested came from planned cavern sites in the domes of West Hackberry and Bayou Choctaw in Louisiana, and from the Bryan Mound dome in Texas. Detailed site descriptions are given in three comprehensive site-characterization reports [14-16]. Textural, mineralogical, and chemical characterizations are based on (1) mesoscopic core inspections, (2) examinations of thick and thin sections, (3) compositional analyses by

means of dissolutioning and x-ray diffraction, and (4) trace-element studies using atomic absorption and microprobe analyses [17-20].

West Hackberry (WH) samples for creep tests were prepared from core from two drillholes: 6C at the depth of 2220-2241 ft, and 108 at the depths 2267 and 3652 ft. The two drillholes are located approximately 3500 f-t apart, some 1000 ft from the north and south edges of the dome, on the 2000-A contour line. In what follows, both drillhole number and depth are used as sample identifiers together with the site abbreviation in the form WH 108-2267, for example.

Specimens from drillhole WH 6C were light to medium-gray and contained bands dark gray, approximately 2 in. wide. The bands contained distinct inclusions to finely distributed impurities. Chemical tests identified all impurities as anhydrite. Medium-to-coarse grains had the greatest dimensions between 0.25 in. and 1.2 in. and were mostly elongated with aspect ratios between 1.5 and 3.5. Impure band and grain orientations were approximately 15° from the core axis. Half of the core 108-2267 consisted of extremely coarse, euhedral grains next to medium-gray material of medium grain size. The salt with medium grain size appeared to contain uniformily distributed, fine second phases. The dividing line between the two materials was nearly parallel to the core axis.The core 108-3652 was entirely coarse-grained with individual grain sizes to 2 in.

Bryan Mound Salt samples came from drillholes 107C at depths of 2506 to 2517 ft; 108B at a depth of 3324 ft; and from 113 at a depth of 4225 ft. Earlier creep experiments were carried out on core from drillhole 107A. Drillholes 107A,C and 108B are near the center of the Bryan Mound cavern array near the center of the dome. Drillhole 113 is in the southeast corner of the cavern field approximately 1500 ft away from the edge of the dome, at the 1500-ft contour line.

Samples from drillhole 107C were white to medium-gray. The darker color was again due to veins of a hard second phase or bands of halite with finely disseminated impurities. The bands were 0.2 to 1 in. wide, 0.23 to 0.4 in. apart, and nearly parallel to the core axes. Samples from 107C had a nonuniform grain size ranging from 0.08 in. to 1 in. Large subhedral grains were common, particularly away from the impure halite bands. Medium-to-fine grain sizes were more typical for material between the bands. The sample 108B-3324 of this study had a more uniform medium-to-coarse grain size and contained only two very thin (<0.08 in.) impurity bands. In general, impurity bands in core from 108B were spaced farther apart than in 107C. None of the core tested from Bryan Mound showed any grain elongation or preferred grain orientation.

Only one Bayou Choctaw sample, 19A-2577, was tested for creep. The sample came from drillhole 19A 700 ft from the southern edge of the dome. The sample was medium-grained, with a few large subhedral grains up to .75 in. It was free of the "banding" common in both West Hackberry and Bryan Mound salt. The sample was light to medium gray.

All of the salt studied was relatively pure halite. Anhydrite, the only bulk impurity identified, occurred in distinct euhedral grains with grain sizes ranging from tens to hundreds of microns ($\approx$ 0.004 to 0.020 in.). Anhydrite crystals were spread uniformily

through halite grains, not concentrated at grain boundaries. Dark veins in some samples above were zones of concentrated anhydrite. Total anhydrite contents in the salt from the three domes varied between 0.5% and **11.4%.** However, analyses of end pieces of the samples that were actually tested in creep indicate that the greatest anhydrite content relevant here **was 7%** for WH108-3652.5. Other core, excluding BM **113,** appeared to contain no more than 4.2% anhydrite. No brine inclusions were seen, but Bryan Mound core from drillholes 107A,C appeared to contain traces of sylvite [17,18].

Atomic absorption and microprobe data [18,19] were consistent with all earlier compositional measurements [17]. Concentrations were determined for Ca, Mg, and **K.** Ca was present in amounts on the order of parts per thousand throughout. K was present in concentrations up to 52 ppm in West Hackberry and Bayou Choctaw salt, and in concentrations between 350 and 780 ppm in salt from Bryan Mound. Mg was generally absent within the sensitivity of the measurements. Microprobe studies of regions of pure halite were unsuccessful in that concentrations of trace elements fell below the detection limit of approximately **1000** ppm. Therefore, it is impossible to say whether any calcium or potassium existed in solid solution within the sodium-chloride lattice, or whether they were mineral bound, e.g. in anhydrite and sylvite.

3 Experiments

Tests were conducted in several large-sample, triaxial creep apparatus for use to **10,000** psi and 250°C. A schematic of the equipment is shown in Figure **1.** The important design features and capabilities are **(1)** it accommodates specimens up to 4 in. in diameter and 8.25 in. in length, (2) it permits separate hydrostatic and deviatoric loading, and (3) it permits compression as well as extension experiments. In addition, (4) samples can be vented at both ends, (5) both axial and radial strains can be measured, and (6) temperature is monitored simultaneously at four locations [10].

Load on the deviatoric loading piston (Figure 1) is regulated with 5-gal accumulators or by means of an electrohydraulic control system. Confining pressure is applied by means of a screw-driven hydraulic actuator. In a leak-tight system, this actuator is also used as a dilatometer [1].

Force and confining pressure are measured externally by means of standard strain-gage-type transducers. Axial deformation is also measured externally by using two diametrically opposed Linear Variable Differential Transformers (LVDTs). Radial deformation is determined either dilatometrically or by means of one or two clip-on transducers. Finally, temperature is monitored simultaneously at four locations: in the wall of the pressure vessel (Figure 1), above the zone heater in the loading ram (Figure 1), and along the specimen axis $\approx$0.75 in. away from each sample end.

Sample preparation, the experiments themselves, the accuracy of measurements, and subsequent data reductions are described in detail elsewhere [12]. However, it is

reiterated that creep tests were carried out under approximately constant stress. This is accomplished by means of frequent updates of the force that is transmitted by the loading piston (Figure 1). Load adjustments are calculated from measured changes in specimen diameter with time or, most often, by postulating that the sample volume remains constant. The latter implies that the deformed cross-sectional area of a specimen in triaxial compression is

$$A_n \approx [2\,exp(\frac{e_1}{2}) - 1]A_0 \approx -A_0 \ln(1 - \frac{\Delta L}{L}) \tag{4}$$

where A_0 equals the cross-sectional area of the sample at the beginning of the test stage. The quantities e_1, L_0, and AL denote the greatest (axial) natural compressive strain, the sample length at the beginning of a test stage, and the change in sample length during the same test stage. Eq (2) is approximately valid because primary and secondary creep of salt are rarely associated with volume increases exceeding 2% or 3% [10].

Note that changes in stress or temperature, either during initial loading or between tests stages for individual samples, are made as rapidly as possible. This means that stress changes take between 2 and 12 seconds, depending on the magnitude of the stress change. In turn, temperature changes take approximately 1 hour per 20°C. Thus, stress changes are almost "instantaneous", at least for small stress changes. Temperature changes, on the other hand, are inevitably slow because of the large thermal mass of a large specimen and massive surrounding hardware.

4 Measurements of Steady State Creep

Figures 2a and 2b show typical creep curves that are obtained depending on whether the creep stress τ is reached from a lower stress τ -AT or from a higher stress $\tau = \tau + \mathbf{AT}$. In both cases, rates of steady state creep, i.e., constant creep rates, are preceded by transients because of work hardening or recovery [21]. It is relatively easy to determine when these processes are balanced at high strain rates ($\geq 10^{-8}$ s^{-1}), either from direct visual inspection of the strain-time records or using numerical data fits, semilogarithmic plots of strain rate versus strain, or double-logarithmic plots of strain versus time [10,12,22]. However, all these methods become ambiguous and unreliable at strain rates less than, approximately 10^{-8} s^{-1}. Contrary to earlier indications, this difficulty is not alleviated by numerical fitting procedures, as indicated in Figure 3. Here, the fitted steady state creep rates were a function of test duration [23]. When this correlation was first discovered, it was disturbing that the trend of the data did not suggest any asymptotic value. Thus, the possibility arose that all steady state creep rates, and the steady state creep models that were determined from these data, were grossly in error.

Three procedures were evaluated to improve the reliability of measurements of steady state creep. Because Figure 3 suggested that transient creep may last much longer than first thought, all three approaches are aimed not so much at determining exact values of

the true rates of steady state creep as at establishing upper and lower bounds. This is done by inspecting transients after changes in stress or temperature, and by comparing maximum and minimum strain rates after such changes are implemented at various strains. Two of the methods entail stress changes, either increases in stress or stress drops. The third approach employs changes in temperature. All three techniques rely on the association of steady state creep with a constant substructure and the fact that creep transients are caused by and indicative of changes in substructure. If creep is climb-controlled, for example, the principal substructural features are the size of subgrains, the free dislocation densities, and the dislocation densities in the subgrain walls.

The types of transients that have been observed for salt are the same as those shown schematically in Figure 2. If the stress is increased (Figure 2a), normal transients are produced that are characterized by creep deceleration caused by hardening. If the stress is decreased, the result is either a normal transient or a complex transient (but ultimately inverse transient), depending on the substructure of the salt prior to unloading and on the magnitude of the stress drop (Figure 2b) [8,21,24-26]. Note that inverse transients are defined as creep records with increasing creep rates as a function of time or strain regardless of the sign and value of the creep rate immediately and shortly after the stress was lowered. The acceleration that is associated with inverse transients of the type discussed here is caused by recovery of the substructure, i.e., softening and adjustment to the stable, steady state structure at the lower stress [21,22,24-26]. Within the context of this paper, inverse transients caused by tertiary creep are excluded.

The important observations from Figure 2 are that hardening and creep deceleration occur if the initial creep rate is still higher than the rate of steady state creep. In turn, recovery with attendant creep acceleration occurs if the creep rate lies below the rate of steady state creep for the prevailing stress. Clearly, if the creep rate at any stress is approached both from a softer and from a harder state, then the observed creep rates would constitute upper and lower bounds of the true rates of steady state creep. It remains only to ensure that the two bounds are not unacceptably far apart. This is done by allowing sufficient strain to accrue before the first stress excursion, by limiting the magnitude of the stress changes, and by repeating the stress excursions, if necessary. Figure 4 shows an example of a typical stress change experiment. First, several percent of strain were allowed to accumulate to obtain a reasonable upper bound, $\dot{e}_{su}$, of the true steady state creep rate at τ = 2410 psi and T = 100.2°C. The creep stress was then increased to $\tau + \Delta\tau$ = 2602 psi (an increase of only 8%) with little additional strain. This procedure limited the danger of activating another mechanism and of producing excessive hardening at the higher stress. Finally, to obtain the desired lower bound of the rate of steady state creep at τ, the stress change $\Delta\tau$ was reversed after approximately six hours. In this particular test, $\dot{e}_{sl}$ was obtained after only one pair of stress changes because the transient upon unloading back to τ was an inverse transient. If the transient had been normal, one or more additional stress changes would have been required until alteration of the character of the unloading transient.

The description of characteristic transients for salt implied that temperature changes have the same effect as stress. This proved true at temperatures up to 120°C as indicated by the distinct transients in Figure 5. Above 120°C transients became less developed at

higher temperatures until no transients were discerned at 160°C. Thus, experiments at low temperatures of $T \leq 120$°C at least, could be used directly, much like stress change experiments, to establish upper and lower bounds of the true rate of steady state creep of rock salt. This was particularly true if relatively small temperature changes were effected to minimize chances of crossing any sharp boundaries between deformation mechanisms. All SPR test's fall into the low-temperature range of creep.

The initial presence of transients with changes in temperature was unexpected. Based on the common notion that the creep of sodium chloride is diffusion-controlled even at ambient temperature ($T = 0.3T_m$; $T_m \equiv$ absolute melting temperature) [1,5,7,27], the substructure of salt was thought to be independent of temperature. Therefore, no transients, (i.e., no microstructural changes) should result with changes in temperature once steady state creep is established [28]. Given this reasoning, temperature change tests were originally viewed primarily as a means of (1) accelerating substructural adjustments towards steady state by going to higher temperatures, and (2) evaluating whether steady state conditions were attained upon return to the lower temperatures of interest. This was to be achieved as follows. If creep was faster than at steady state at some temperature T, then a temperature increase, AT, should have resulted in a readily identifiable normal transient with creep deceleration toward the proper rate of steady state creep. After lowering the temperature back to the starting temperature T, the creep rate should have been constant if the true rate of steady state creep was reached at T + AT. If further creep deceleration was noticed at T, the temperature excursion from T to T + AT and back to T could have been repeated. Alternatively, because it is difficult to demonstrate the lack of any transient over noise at low strain rates, the minimum creep rate at T after the first temperature cycle through $T + \Delta T$ could have been accepted as an improved upper bound of the steady state creep rate.

The third approach to determining rates of steady state creep is demonstrated in Figure 6, in combination with more temperature change tests. Here only stress decreases were used to avoid substructural changes that might result with increases in stress. In this case, we attempted to identify the development of steady state creep by determining when transients following stress drops no longer changed with straining at the reference stress. Although promising in principle, this idea proved less workable because it mandated exceptionally accurate stress control under all conditions, and resolution of strain rates down to at least $10^{-10}s^{-1}$. The method is still used in "stress dip" experiments to estimate the magnitude of "back stresses" [21,26], but it was abandoned for the evaluation of steady state creep in favor of temperature change tests.

5 Test Matrices

The test matrices for salt samples from West Hackberry, Bryan Mound, and Bayou Choctaw are listed in Appendix A, Tables Al-A3 in terms of nominal stress (f25 psi), nominal temperature ($\pm.2$°C), and sample source. All experiments were conducted in tri-

axial compression. Previous comparisons demonstrated that the measurements in triaxial compression, which are easiest, also apply to triaxial extension [3].

Note that) shear stress is defined as the maximum difference in principal stresses. The range of shear stresses $\tau = (\sigma_1 - \sigma_3)$ varied between **1830** and **3270** psi. However, measurements of steady state creep were restricted to stresses above approximately **2000** psi. The stress of **1830** psi in Bayou Choctaw tests was chosen only to monitor recovery as a function of accumulated creep strain at 2000 psi. Temperature was varied between 22°C and 80°C. The test temperature of 60°C was preferred because it corresponds to the in *situ* rock temperature at most cavern sites. Tests on Bryan Mound sample BM108B-3324 were carried out at a confining pressure of 500 and 3000 psi. The confining pressure was **2000** psi in all other tests.

6 Results

The exact parameters and the results of **54** tests on eight samples are summarized in Appendix B, Tables B1-B9. The tables include the test durations and the magnitudes of the greatest (axial) compressive strains, e_1. The creep rates $\dot{e}_{1b}$, $\dot{e}_{1e}$ are best estimates of the creep rates at the beginning and at the end of each test. They are either secant slopes or slopes of linear least-squares fits to subsets of the measurements as defined in Appendix B. The values for $\dot{e}_{1e}$ are the upper and lower bounds of steady state creep that were discussed in the previous section. Note that the shear strain rates, $\dot{\gamma}$, that are used in constitutive models, are $\approx \frac{3}{2}\dot{e}_1$, neglecting comparatively small volumetric strains, e $(\frac{e}{\gamma} \leq 0.1)$ [3,4,10,11].

The complete creep curves from which the average stresses, strains, and strain rates are taken in the tables of Appendix B are included as Appendix C. The records for West Hackberry sample (WH) 108-3657.5 and for Bryan Mound samples (BM) 107C-2516 and 108B-3324 are relatively rough because they were taken before major improvements were completed in the methods used to control both the confining pressure and the ram load (Figure **1).** Figure 6, which was presented earlier, is a section of Figure C9. Note the enlargement of Figure C2a in Figure C2b to demonstrate the recovery transients following stress decreases. Fig. C2a also shows two vertical bars towards the end of test stage **1.** They define the bounds of the interval for determining $\dot{e}_{1e}$ by means of a linear least-squares fit (last column in all tables in Appendix B).

Results of earlier creep measurements on salt from West Hackberry and Bryan Mound are reproduced in Appendix D [3,4]. These results were used in several fits combined with the new data of Appendix B.

Some general comments concerning the appendices are included in the title pages for each group. For example, the title page for Appendix B describes exactly how the strain rates $\dot{e}_{1b}$ and $\dot{e}_{1e}$ were determined.

6.1 Analysis of Steady State Creep

6.1.1 Power-Law Model

Several investigations have demonstrated the agreement between power-law creep models, Eq (3), and estimates of steady state creep for rock salt from at least five different sites, including domal and bedded-salt formations. Therefore, power-law creep was also assumed to hold in earlier work on salt from West Hackberry and Bryan Mound, and sparse data were interpreted accordingly. The extra data in Tables B3-B5 permit a more thorough evaluation of the relevant parameters. A nonlinear least-squares-fitting procedure together with a shear modulus $\mu = 1.8 \times 10^6$ psi and R = 1.986 (cal/mole degree) [29] was used to obtain power-law stress exponents n, effective activation energies Q and structure (preexponential) factors C for the following groups of data. (1) Estimates of steady state creep following stress increases, (2) estimates of steady state creep including and excluding earlier measurements into the fits, and (3) estimates of steady state creep or, more accurately, creep rates after stress drops. The results obtained are listed in Table 1 together with the standard errors, SE, of the logarithm of all fits. Note that separate fitting parameters were determined for the creep measurements on salt from drillhole BM113 because this salt exhibited behavior distinctly different from that of other salt from the same site. Table 1 includes fits to two larger data sets for Salado salt. The set WIPP4C was used extensively as a reference for earlier creep measurements in support of SPR. The set WIPP7 is a new and smaller but improved set of measurements of steady state creep that were determined in stress and temperature-change tests.

Note that the fitting parameters above for the data sets BM3C, BM4C, and WIPP7 in Table 1 (data group 1 above) are based on upper and lower bound rates of steady state creep. If only upper bound values were available, then only the smallest values were included for each test stage and sample. In turn, the data sets WH4 and WH5 in Table 1 (data group 3 above) are believed to be only lower bounds of the rates of steady state creep associated with inverse transients after stress decreases. Beyond this selection of data, the 22°C measurements for Bryan Mound salt were excluded throughout because the creep rates at that temperature appeared to lie well below steady state values. This was indicated by insufficient transient creep compared to much larger transients in other tests; for example, QD11AN (Table B1), QF37N (Table B8), and especially QG4N (Table B9). The rejection of the 22°C data is also supported by the plot of the logarithm of temperature-compensated creep rate, $\dot{e}_{1e} \exp(Q/RT)$, versus the logarithm of stress in Figure 7 using the Bryan Mound data of Appendix B. The questionable points enclosed in a circle fall outside the range of all other measurements.

Note that all underlined values in Table 1 were prescribed and held constant. This was done, for example, to obtain power-law stress exponents if the effective activation energy in Eq (3) was set equal to the activation energy of core-diffusion for Cl-, which should be the slowest moving species during climb-controlled creep [30]. Similarly, n and = Q were constrained to 4.9 and 12.0 kcal/mole to evaluate the significance of the differences

in fitting parameters of the present data to the fitting parameters of earlier data sets for Salado salt and West Hackberry salt. Note also that the standard error decreased for some of the constrained fits. This fact, which is not obvious, is a consequence of the small number of measurements in several of the data sets. As a result, the standard error for some fits to those sets becomes unduly sensitive to the number of degrees of freedom (number of measurements minus the number of constraints) involved. This sensitivity indicates that the relative magnitudes of standard errors cannot always be used as a discriminant for the quality of alternate equations [31].

Figures 8a to 8e show the individual data within each data set that were included into the fits for West Hackberry, Bryan Mound, Bayou Choctaw and Salado salt. Figure 8e is a superposition of the fits in Figures 8a-d.

6.1.2 Alternate Models

Power-law fits yielded excellent description of creep data over the ranges of stresses and temperatures that are similar to the conditions of this study [1,5-7,22,27,32,33]. This observation is clearly supported by small standard errors of fits in Table 1, especially for West Hackberry data sets WH1 and WH2 and for Bryan Mound measurements BM4C on core BM113-4225. Both of these data sets exhibit relatively little scatter. The good quality of power law fits coupled with power law-stress exponents around 5 appears to imply that the creep of salt is diffusion-controlled even at low temperature ($T \approx 0.3T_m$ [1,13,22,24,25,27,28,32,33]. Both good fits and the knowledge of the rate-controlling deformation mechanism are then used to justify the extrapolation of the power-law fits to much lower stresses than those of the underlying experiments. Some recent experimental evidence suggests that this procedure should be followed with caution, mainly because the mechanistic interpretation of many power-law fits is not definitive. Inexplicably low effective activation energies, Q, large activation areas in rigorous activation analyses, creep transients after temperature changes during or close to steady state creep and

deformation process. Therefore, if power-law fits are only approximations to the true creep phenomena, it is reasonable to evaluate alternate models. Candidate models for the

[34-41]

$$\dot{e}_1 = B_1 exp\left(-\frac{B_2}{RT}\left(B_3 - \ln\frac{\tau}{\mu}\right)\right), \tag{5}$$

$$\dot{e}_1 = B_1\left(\frac{\tau(1-B_7)}{\mu}\right)^{B_2} exp\left(-\frac{1}{RT}\left(B_3 - V\tau(1-B_6)\right)\right) \tag{6}$$

where

$$V = B_4 exp\left(\frac{-B_5}{RT}\right).$$

As a further alternative, $\tau(1 - B_6)$ was replaced by $(\tau(1 - B_6))^{B_8}$. As before, μ is the shear modulus, T is temperature, and $\tau = (\sigma_1 - \sigma_3)$ is the shear stress. B_2 in Eq (5) and B_3 in Eq (6) are activation energies. In contrast, $B_3 = \ln(\frac{\tau_0}{\mu_0})$ in Eq (5). τ_0 and μ_0 are the flow stress and the shear modulus at absolute zero. V denotes an activation volume.

Note that the constants B_2 and B_3 in Eqs (5) and (6) do not have the same physical significance. The equal designation of these two constants merely facilitated the tabulation of fitting parameters.

Equation (5) is a model for cross-slip [34,35,41], and B_2 represents the activation energy for cross-slip, Q_{CS}. Equation (6) is the general model for glide, dislocation intersection, and climb in the presence of back stresses. If $B_4 = B_5 = B_6 = 0$, Eq (6) reduces to the modified power law for which B_7 represents an internal back stress [21,26,42]. A back stress was introduced into the conventional power law when large stress exponents, $n = B_2 > 5$ were observed [42]. It was found that the stress exponents could be reduced to between 3 and 4 if the back stress was allowed to decrease with increasing applied stress. More recent data for aluminum, stainless steel, and rock salt indicate that the backstress is instead directly proportional to the applied stress [43-45]. $B_5 = B_6 = B_7 = 0$ in Eq (6) corresponds to the most common dislocation glide model. Other combinations of fitting parameters yield alternate glide and intersection models. The form of the temperature dependence of the activation volume, V, was suggested by data for magnesium [46]. If the temperature dependence of the activation volume V is offset by the multiplier $\frac{1}{T}$, then Eq (6) reduces to the empirical stress dependency $exp(\alpha\tau)$ used by Heard for artificial polycrystalline halite [39].

The applicability of the models, Eqs (5) and (6), was evaluated in two ways. First, several parameter combinations and standard errors were determined again by means of nonlinear least-squares fitting. To make this fitting procedure more meaningful, it was also applied to two larger data sets for rock salt from the Salado formation. Selected results of the various fitting processes are summarized in Table 2. Abnormalities in the quality of some fits appear to be indicated again when the standard error for Eq (6) increases with an increase in fitting parameters. As mentioned in the previous section, this problem relates to the strong influence of the number of degrees of freedom of particular fits when the number of measurements involved is small. Therefore, the standard error becomes dominated by the variance of these fits about the regression compared to the variance due to the regression [31]. In these cases, comparably large standard errors do not necessarily indicate the inappropriateness of a more complex fitting function.

The exponential forms of Eqs (3) and (5) imply linear relationships between the quantities $\ln \dot{e}_1$, $\ln \tau$ and $\ln \dot{e}_1$, 1/T. This means that the creep parameters Q, n, and Q_{CS} are related according to

$$n = \frac{Q_{CS}}{R\,T}$$

$$Q = Q_{CS}(\ln \frac{\tau_0}{\mu_0} - \ln \frac{\tau}{\mu}). \qquad (7)$$

It also means that diffusional creep and cross-slip might be distinguished by determining whether the power-law stress exponent, n, and the effective activation energy, Q, are really constant, or whether they are a function of temperature and stress, respectively. This possibility was indicated earlier by data correlations for Salado salt, file WIPP7 in Table 2. To verify this observation, the second approach to model discrimination here consisted of careful experiments on Bryan Mound salt BM113-4225 at two stresses and temperatures. The results for temperatures of 40°, 60°, and 80°C are plotted in Figure 9 using the best estimates of steady state creep in Table B8. Obviously, the results are inconclusive. The 80°C estimates of steady state creep $\dot{e}_{1e}$ might be larger than true steady values, thus yielding a very low power-law stress exponent [47]. The value n = 7.13 also looks unusual although it cannot be dismissed unless the present criteria for the identification of steady state creep are abandoned. By these criteria, the creep rate $\dot{e}_{1e}$ at τ = 2488 psi is an upper bound estimate of the true rate of steady state creep because it follows a normal transient. In turn, the values $\dot{e}_{1e}$ at the stresses 1836 psi and 2844 psi are upper and lower bound estimates of steady state creep. If they are normalized with respect to the same temperature, then the latter two estimates are, in fact, identical.

6.2 Activation Analyses

The identification of the governing mechanism of creep is often based on the match between measurements (or estimates) of steady state creep and a particular model, for example Eq (3), out of a choice of models such as Eqs (5) and (6). The fits in Table 1 do not guarantee a correct physical interpretation of the data. Therefore, as mentioned previously, Eq (3) can be taken as credible evidence for dislocation climb only if the fitted values of the stress exponent and the effective activation energy agree with theoretical predictions and independent diffusivity measurements. Given the limited data base and the uncertainty concerning the comparative quality of the fits in Tables 1 and 2, recourse was also made to activation analyses,

Because salt creep is thermally activated, each creep process, i, obeys the general rate equation for both transient and steady state creep [36-39]

$$\dot{e}_{1i} = D_i(\tau, e_1, T)exp(-\Delta G_i/RT). \tag{8}$$

D_i is a "structure term" that depends, among other factors, on the number and arrangement of dislocations and on their vibrational frequency, on grain size and on the type and distribution of impurities. ΔG_i is the change of the Gibbs free energy of the system if a dislocation is moved to the saddle point between adjacent equilibrium positions. Physically, ΔG_i is a measure of the resistance of particular types of obstacles to dislocation motion. Obstacles can often be identified, noting that the Gibbs free energy is the sum of the activation enthalpy and an activation entropy term:

$$\Delta G_i = \Delta H_i - T\Delta S_i. \tag{9}$$

Because

$$\Delta H_i = \Delta H_{0i} - A_i b \tau_e, \tag{10}$$

Eq (8) can also be written as

$$e_{1i} = D_i(\tau, e_{1i}, T) exp(\frac{\text{AH; } - \text{ TAS;})}{RT})$$

$$= D_i' exp\left[-\frac{(\Delta H_{0i} - A_i b \tau_e)}{RT}\right] \tag{11}$$

where ΔH_{0i} denote activation enthalpies at absolute zero. In the notation of Eqs **(10)** and **(11)**, the ΔH_{0i} include mean stress-volume terms. Within the context of this study, these latter terms are negligible. A_i and b are activation areas and the Burgers vector. The parameters ΔH_i, A_i, etc. are characteristic for each process and are called activation parameters. If it is assumed that one of these processes is rate-controlling under particular conditions of stress and temperature, then only one set of values ΔS_i, ΔH_i, . . . remains and the subscript "i" may be dropped.

Note that τ_e here is understood to equal the difference between the applied stress, τ and a long range internal back stress, τ_b, i.e.,

$$\tau_e = \tau_{effective} = (\tau - \tau_b). \tag{12}$$

τ_b corresponds to the fitting parameters B_6 and B_7 in Eq (6). Ab in Eqs **(10)** and **(11)** corresponds to the activation volume V in Eq (6).

To identify a dominant mechanism requires determining the activation enthalpy, AH, and the activation area, A. In this study, approximate values for both parameters were obtained by correlating the pairs of creep rates, $(\dot{e}_1)_2$ and $(\dot{e}_1)_1$, that were measured right before and after changes in stress and temperature. In both cases it was assumed that B_1 and the back stresses did not change "instantaneously" with the applied stress and temperature and that the obstacle structure was associated with well-defined saddle points in the Gibbs free energy profile. Therefore,

$$\text{AH} = -R\frac{\delta \ln \dot{e}_{s_1}}{\delta(\frac{1}{T})}|_\tau \approx -\text{R}\frac{\ln \frac{(\dot{e}_1)_2}{(e_1)_1}}{\frac{1}{T_2} - \frac{1}{T_1}}|_\tau \tag{13}$$

and

$$\text{A} = \frac{\text{RT}}{\text{b}} \frac{\delta \ln \dot{e}_1}{\delta \tau}|_T$$

$$= \frac{\text{RT}}{b\tau} \frac{\delta \ln \dot{e}_1}{\delta \ln \tau}|_T \approx \frac{RT}{b\tau} \frac{\ln \frac{(e_1)_2}{(e_1)_1}}{\ln \frac{\tau_2}{\tau_1}}, T. \tag{14}$$

Note that the strain rates, $(\dot{e}_1)_2$ and $(\dot{e}_1)_1$ in Eqs **(13)** and **(14)** do not need to be steady state strain rates. Some values for AH and A are listed in Table 3. Values for A are given in terms of multiples of the square of the Burgers vector, b.

In general, the activation enthalpy AH, Eq (13), differs from the effective activation energy Q of the power-law model, Eq (3). The value of Q is obtained from individual data pairs by replacing the creep rates $(\dot{e}_1)_2$, $(\dot{e}_1)_1$ with the corresponding steady state creep rates, $(\dot{e}_{1s})_2$, $(\dot{e}_{1s})_1$. The difference between the activation area A and the power-law stress exponent n is more pronounced. The value of A is derived under the assumption of zero change in structure, i.e., $\delta D'/\delta\tau = 0$. In turn, the validity of the power-law, Eq (3), assumes that the term $Ab\tau$ is negligible compared to the activation enthalpy ΔH_0 (i.e., AH $\approx$ Q), and that the stress exponent n can be determined from the structure term D' during steady state creep. Thus

$$n = \frac{\delta \ln \dot{e}_{1s}}{\delta \ln \tau}\Big|_T. \tag{15}$$

With these assumptions, n is usually obtained by means of a single fit to all available measurements of steady state creep as in Table **1** and Figure 8. In some cases, however, detailed activation analyses include the determination of n-values from individual pairs of measurements associated with stress changes from τ_1 to τ_2,

$$n \approx \frac{\ln \frac{(\dot{e}_1)_2}{(\dot{e}_1)_1}}{\ln \frac{\tau_2}{\tau_1}}\Big|_T. \tag{16}$$

This procedure was followed here (Table 3) to isolate possible trends in values resulting from different combinations of upper and lower bounds of the rates of steady state creep in the Tables of Appendix B.

6.3 Creep After Stress Drops

Some uncertainty surrounds the creep behavior of rock salt after stress reductions. Assuming that steady state creep is a function of state, then by definition it should be independent of stress, temperature, and microstructural histories. This tenet is substantiated by some (but not all) creep measurements on NaCl, and other materials at high temperature [22,24-27,39,48-54]. However, even if steady state creep is unique, stress change tests, constant strain rate experiments and recent microstructural evidence suggest [25,39,51,52] that transient creep associated with stress reductions may be relatively large. An example is 3% to 6% for sodium chloride single crystals when the stress is decreased to half its starting value at 615°C [25]. Such strains correspond to very long times at strain rates of $10^{-9}\,s^{-1}$ or less. As a result, conditions arise when transient creep may dominate. This problem was demonstrated by an experiment where the creep of rock salt was measured at 2920 psi before and after creep at 4440 psi [10]. Figure **10** shows

that the creep rate during stage 3 of this test was almost 10 times smaller than at the end of stage 1. Equally important, any creep recovery during stage 3, if it existed, was too slow to be resolved during 700 hours.

The problem of creep and recovery after stress reductions was partially addressed in experiments on rock salt from West Hackberry and Bayou Choctaw and in parallel exploratory tests on salt from the Salado formation, New Mexico. The first set of multistage tests compared the creep rates of two West Hackberry samples in stress increment tests and in stress drop tests at 60°C between 1970 and 3010 psi. The exact stress conditions and the results of both sets of tests are summarized in Tables Bl and B2. The actual creep records are shown in Fig. Cl and C2. Since both sets of experiments preceded the adoption of more systematic temperature change tests to bound steady state creep rates, several criteria were used to determine the duration of each test stage. For example, stage 1 in test QD12AN (Table Bl) was run for the same duration as typical earlier tests on Salado salt that served as references for this SPR study. It was not clear at that time that the creep rate at the end of that stage might be considerably greater than the true rate of steady state creep. The duration of stage 1 in Table B2 was predetermined to correspond to approximately 10% strain. Stage 2 in Table B2 was ended because the creep rate appeared to be constant following the pronounced inverse transient for some 50 hours after the stress drop. Stages 3-5 of Table B2 were terminated because no change in creep rate was detected , specifically no creep acceleration. Stage 5 in Table B2 was added to amplify any possible evidence for recovery at a higher temperature, as indicated by an inverse transient in the last section of the plot in Figure C2.

Table 1 compares the fits to the data in Tables Bl and B2. Distinctly different fits were obtained depending on whether the data were based on loading (stress increment) or on unloading (stress decrement). This is also shown in Figure 11. The "unloading" slope n = 14.25 was obtained without the datum of stage 5 in Table Bl. Observations of this kind are consistent with some reports that dislocation arrangements in subgrains, specifically subgrain size in sodium chloride and in some metals, is dictated by the highest stress [27,48,49,53]. However, the significance of Figure 11 hinges on whether or not the present unloading measurements represent steady state values. Two indications suggest that they do not. First, the stress drop at the end of stage 5 in Table Bl was followed by a distinct inverse transient. Such a transient is direct evidence for recovery (Le., structural readjustments towards a "softer" structure at the lower stress) unless the transient resulted from true tertiary creep with impending creep rupture. Unfortunately, the latter possibility cannot be ruled out completely, because the creep rate at the end of stage 6 was higher than the creep rate at the end of stage 4 (Table Bl). An instability, of course, would invalidate the measurement during stage 5 within the context of steady state creep. At the same time, the nature of a possible instability remains puzzling because the creep rate during stage 6 did not continue to accelerate beyond the sharp initial transient. Also, the creep during the preceding stage 4, agreed quite well with the corresponding measurement for stage 1 in Table B2. The latter observations suggest that the creep rate for stage 5 of test QD12AN may well be a good measurement.

A second observation relates to the inverse transient caused by the increase in temperature from 60°C to 80°C during stage 5 of test QD11AN in Figure C2 and Table

B2. The existence of this transient is taken as unambiguous evidence that the creep rate at the end of stage 4 and (probably) during stages 3 and 4 were smaller than the true steady state creep rates at these stresses.

Comparison of the strain accumulations during the various stages in Tables Bl and B2 reveals that the sample in Table B1, QD12AN, underwent less strain at the highest stress, $\tau \approx 3000$ psi, than the sample in Table **B2, QDllAN.** Therefore, it is reasonable to expect that QD12AN would have recovered to a steady state creep rate sooner and after less strain than did **QDllAN.** Another set of experiments was conducted to pursue this reasoning without the possible interference of tertiary creep. First, bounds of the steady state creep rate were established at $\tau = 2100$ psi and 60°C for a salt sample from Bayou Choctaw, Table B9. Then the specimen was subjected to a nominally 12% higher stress for 2, 24, and 407 hours. After each interval the stress was dropped back to the "reference" value to monitor the effect of the higher stress on the shape of the creep curve and on the magnitude of the creep rate as a function of time and strain. This sequence of experiments covered the stages 7 through **13** in Table B9. The data in Table B9 show that the creep rate at the reference stress decreased rapidly with an increase in strain, i.e., hardening at the higher stress. Even the small strain accumulation of 0.075% during stage 8 produced a nearly twofold reduction of the creep rate after 266 hours at the end of stage 9. However, the creep rates after the stress reductions were so low throughout that it was impossible to complete the consecutive recovery processes as hoped. In this case, because of some noise in the measurements, it even proved impossible to resolve any recovery at the low strain rates of the order 10^{-10} s^{-1}. However, the total strain due to recovery during stages 9, **11,** and **13,** equals only about one tenth the strain at the higher stress during stages 8, 10, and 12. Therefore, it is unlikely that the lack of recognizable creep acceleration implies that the steady state creep rate at the "reference" stress was altered. Rather, it might just take a long time to restore the creep rate of the salt sample to that before the first stress increase to $\tau = 2468$ psi.

The third set of recovery tests was similar to the unloading experiments on West Hackberry salt, **QDllAN,** but they included a recovery step at a higher temperature. They also included ongoing observations of substructures before and after recovery. The objectives of these tests were accomplished by cutting a 2-in.-thick section from the middle of a sample at the end of a creep test at $\tau \approx 2900$ psi, by reloading the remaining sample parts, and, finally, by dropping the stress to $\tau \approx 1250$ psi. Results of the second loading phase at $\tau = 2908$ psi and of the recovery measurements at the lower stress at 58°C and 110°C are shown in Figure 12. While the strain rates for this two-part sample may be in error by as much as 50%, recovery appeared to occur relatively quickly at 110°C and after < 0.5% strain.

6.4 Some Substructural Observations

Substructural observations are often used to identify rate-controlling deformation mechanisms in solids and in the establishment of steady state conditions. The principal features of interest in sodium chloride are the concentrations of dislocations in glide

bands, the preferential arrangement of dislocations in low-angle subgrain boundaries, dislocation spacings within boundaries, and the dislocation densities and arrangement between subgrain walls. The dislocations that are not associated with subgrain boundaries are generally referred to as "free" dislocations although not all of them may be mobile. Substructural features, especially well-developed subgrain boundaries have been taken as evidence for diffusion-controlled creep not only above, but also at or below, half the melting temperature of salt [22,24,25,27,48,49]. Moreover, there is evidence that the subgrain 'size, $\overline{d}$, and the free dislocation density of steady state creep are related to the magnitude of the applied stress. Several data sets from laboratory experiments on single crystals and polycrystalline salt, and observations on naturally deformed rock salt indicate that the relationship between subgrain size and stress falls within the range $75\tau^{-1} \leq \overline{d} \leq 255\tau^{-1}$ [25,27]. Following universally accepted convention, subgrain size in this expression is given in micrometer (μm) and stress is given in megaPascals (MPa).

No systematic substructure observations were collected in this study. Nevertheless, a few measurements were made to obtain some indication concerning the mechanistic significance of good power-law correlations for steady state creep. Cursory substructural measurements were also of interest for the consideration of low creep rates for Bryan Mound salt compared to the measurements on salt from West Hackberry.

Substructures were identified in undeformed samples of West Hackberry salt, WH108 at depths of 2293 to 2298 ft, and Bryan Mound, BM107C-2205; and in deformed West Hackberry salt, sample WH108-2267 (Table B2). Representative observations are shown in Figures 13 to 15.

The substructures in laboratory undeformed salt WH108 are shown in Figure 13. The salt consisted of a very well developed, nearly equant and rather uniform subgrain structure with an average subgrain size of 345 μm and relatively small standard deviation, s = 32 μm. The dislocations between quite linear subgrain boundaries are arranged in cellular patterns reminsicent of dislocation arrangements in copper [50]. The initial substructure in Bryan Mound salt from 107C-2205, Figure 14, is irregular by comparison. Although dislocations are concentrated in subgrain boundaries, the sub-boundaries are mostly curved and the subgrain size highly variable. The mean subgrain size is small, a = 115 μm. The variation in subgrain size variation is reflected in a relatively large standard deviation s= 45 μm. A quick check at least indicated that the finer subgrain size of Bryan Mound salt did not appear altered by static annealing under hydrostatic pressure at 160°C for 14 days (Table B7).

Substantially different features appeared in WH108-2267 that was deformed to 9.67% strain at τ = 3010 psi and at 60°C before several stress drops and one temperature excursion to 80°C. The strain during all stress drop tests was only 0.4%. Three representative photographs are included in Figure 15. The substructure in Figure 15a is dominated by glide bands. Figure 15b shows some primarily curved, often open-ended concentrations of dislocations that might be vestiges of a disintegrating subgrain structure. Figure 15c, the third major feature in this sample, may be a newly developing subgrain structure, but is probably wavy slip bands indicative of cross-slip. The latter suggestion is supported by the fact that the etched grooves or boundaries in Figure 12c are only 3 μm or less

apart. If this distance corresponded to the spacing of subboundaries then (for example) the existing stress-subgrain size relationships would indicate a creep stress >7500 psi, which lies well above the maximum 2900 psi in the tests on this sample (Table B2).

7 Discussion

The present study was motivated primarily by pragmatic questions about the appropriate power-law stress exponents for steady state creep of salt from different SPR sites and about any anticipated differences in material properties within each of these sites. To minimize testing it was also important to identify possible reasons for observed differences in creep response of salt from different locations; for example, West Hackberry and Bryan Mound. Knowing the causes might help establish other indicator properties such as a combination of salt texture and composition that could be correlated with mechanical salt properties with less effort and expense than required by creep testing. While addressing these practical questions, however, several broader concerns arose that appear fundamental to the successful application of laboratory data to SPR design calculations.

Prompted by parallel observations on bedded salt from potential sites for radioactive waste disposal, the question arose whether previous measurements for SPR were, in fact, steady state measurements. Therefore, it was not clear whether the power-law fits to earlier data were valid descriptions of the steady state creep of rock salt. If steady state creep had not been attained in the earlier experiments, this also implied that transient creep would last longer and, more important, dominate creep through more strain than previously thought. Hence, there would have to be a concern for when data could be expected to agree with predictions based solely on steady state creep models. The related question concerning the rate of recovery and the duration of transients following decreasing stresses was recognized several years ago. This question has gained in importance because of suggestions that the steady state creep rate of salt at particular service stresses is permanently altered if it is ever loaded to a higher stress. This irrevocable change in creep properties is attributed to a permanent effect of the higher stress on the arrangement and motion of dislocations. If true, this means that "steady state" creep can no longer be described by a state function of the type of Eqs (3), (6) or (8). The last relevant and major concern must be whether constitutive models for laboratory measurements that were made over a narrow range of relatively high stresses can be extrapolated to the low stress conditions around SPR caverns years after they were excavated. This problem is greatest at the typical SPR temperatures near forty percent of the melting temperature of sodium chloride. It is here that the governing deformation mechanisms of salt and, therefore, the most appropriate functional form of a creep law are not well understood.

The difficulty in determining the onset of steady state creep at strain rates below approximately 10^{-8} s^{-1} is well known. The appearance of creep curves and where the

creep rate along such records becomes constant can be deceiving. For example, Figure. C2b shows the tail end of a plot of the first stage of West Hackberry test QD11AN. It looks perfectly straight. However, if all the data for that stage are considered in Figure C2a, then it is apparent that the curve is dominated by transient creep. Similarly, the transient nature of creep towards the end of stage 1 of the test on Bayou Choctaw salt, Figure C9 might be overlooked without the prolonged creep deceleration during stages 2, 4 and 6. The normal transient during these stages persists through more strain than is typical for a 20°C increase in temperature. Therefore, it is not surprising that the upper and lower bound estimates of steady state creep for stages 1 and 7 at τ = 2130 psi are a factor of three apart. This difference is important for the derivation of the governing creep parameters. Generally, the power-law stress exponents and effective activation energies are underestimated if the creep rates used are higher than the true steady state creep rates [47]. This point is demonstrated by means of Eqs (3) and (11), using the creep rates of stages 1, 2, and 7 in Table B9. After the $\dot{e}_{1e}$-values of stages (1,2) and (2,7) are paired, the effective activation enthalpies become Q $\approx$ AH $\approx$ 9.9 and 23.1 kcal/mole. In this case, the Q = 23.1 is an upper bound because the creep rates $\dot{e}_{1e}$ for stages 2 and 7 are believed to be above and below the corresponding true steady state creep rates, respectively. It follows that the mechanistic interpretation of creep measurements based on the magnitudes of measured or inferred activation parameters,e.g., Q or AH, are extremely sensitive to the quality of the available data. The observations for pairs of data carry over to correlating groups of data. We believe that the difference in the overall fits to creep data for Salado salt in Table 1, files WIPP4C and WIPP7, is mainly due to the fact that the set WIPP4C contains only upper bound estimates of steady state creep. This bias in the earlier Salado measurements, WIPP4C, results in appreciable differences in calculated creep rates. If the power-law fits with the lowest standard errors (Table 1) are used, the predicted steady state creep rates for τ = 1000 psi and T = 40°C are 2 $\times 10^{-10}$ and 5.9 $\times 10^{-11}$ s^{-1}. Assuming possible geologic conditions, τ = 150 psi and T = 70°C the extrapolated values are 1.4 $\times 10^{-13}$ and 3.9 $\times 10^{-14}$ s^{-1}. These predictions differ by factors of approximately five. Of course, the latter predictions rest on the assumption that the power-law also describes the governing creep mechanism at the lowest stresses of interest.

All of the West Hackberry tests precede the adoption of systematic temperature change tests described earlier. Therefore, the measurements for West Hackberry salt under this program are only upper bound estimates of steady state creep, and the fits of Table 1 should overpredict the true steady state creep rates of this material. This suggestion is supported by low-power law stress exponents, n, and low effective activation energies, Q, for West Hackberry data sets WH1 and WH2 as compared with the corresponding values for Salado salt, WIPP7, or Bryan Mound salt. The data sets WH1 and WH2 do not include the measurements of stress drop tests.

Although the available creep rates for West Hackberry salt may be somewhat greater than the corresponding true steady state creep rates, it is reassuring that they consistently show very little scatter. Because bedding planes in salt domes are nearly vertical, the reproducibility of data for salt from four different drillholes suggests considerable lateral homogeneity in creep properties. The reproducibility between the results of this study

(Tables B1 and B2) and of earlier tests (Table **D1)** also implies continued validity of the model parameters of past design calculations for SPR at West Hackberry. For example, previous design analyses [55] predicted effective steady state creep rates of 8.46×10^{-9} s^{-1} for σ = 2000 psi and T = 60°C.† This compares with 9.35×10^{-9} s^{-1} for the combination of all existing measurements for West Hackberry salt, data set WH2 in Table 1. Note that the predicted creep rates do not change much for the various parameter combinations in Table **1.** The extrapolated creep rates for the West Hackberry sets beginning with C = 3.30×10^{14} and C = 1.94 X 10^{14} at σ = 500 psi and T = 60°C lie around 10^{-11} s^{-1} and differ by only 20%.

According to Tables B3 through B8, the results for Bryan Mound salt are a mix of upper and lower bound measurements of steady state creep. Although these bounds differ by as much as 500 %, their existence makes it possible to estimate unavoidable uncertainties in creep predictions in situ. Together with Salado data, files WIPP4C and WIPP7, they also yield estimates of the likely uncertainties in material models that are based *only* on measurements of upper bound steady state creep rates.

Although only one sample from Bayou Choctaw was tested, it is clear that the behavior of this salt is similar to that of Bryan Mound salt from drillholes 107A, 107C and 108B. Because of extended transient creep, most of the data for this material are upper bound estimates of steady state creep. This is the reason for the relative low values of the parameters C and n in Table **1.**

During the first creep tests on Bryan Mound salt [4] this material crept considerably slower than any other salt known to us. The present data confirm this observation for all samples except BM113-4225. Because most of the Bryan Mound samples were carried out under well-controlled laboratory conditions, the scatter in the results for drillholes 107A, 107C, and 108B (Tables B2-B8, D2) points to an unusually large variability in the creep properties of this salt. This becomes especially clear from the differences between the measurements for BM113-4225 and the remaining Bryan Mound samples. At this point, the reasons for these unusual characteristics of Bryan Mound are unknown. In principle, the low and highly variable creep rates could be due to intracrystalline secondary phases such as anhydrite. They could also be due to impurities in solid solution.

For example, Ca^{2+} in solid solution can result in large increases in the activation energy in the dislocation climb regime of creep [51]. Unfortunately, no way was found to measure the level of candidate species, calcium, potassium and magnesium in rock salt in this study below a level of appromximately 1000 ppm. Samples for atomic absorption tests appeared to be contaminated with secondary phases; microprobe tests turned out to be too insensitive. In turn, secondary phases are abundant and cause considerable local changes in dislocation substructures. However, they appear to be spaced too far apart to dominate the substructure and the average creep rate of our specimens.

The effects of differences in the initial substructures, especially subgrain sizes in

†The definition of effective strain, $\dot{\varepsilon}$, in SPR analyses is such that $\dot{\varepsilon} = \dot{\varepsilon}_{1c}$ under the axisymmetric conditions of triaxial laboratory tests.

laboratory undeformed salt from different locations, were also considered. Although the subgrain size for Bryan Mound salt $\bar{d}$ = 115 pm, is small, it is still coarser than the equilibrium subgrain size for the stress levels of this study. According to studies of Blum, Poirier, Carter, and others, the subgrain size at the lowest stress level for Bryan Mound salt, σ = 1800 psi, should be less than approximately $\bar{d}$ = 25 pm. For this reason it is likely that substructural differences will alter only the magnitudes of the transient creep strains that are measured for different salt types, but not the rates of steady state creep. As three last possibilities, the effects of texture, grain boundary impurities, and of water should be evaluated. This has not been done to date, because available laboratory creep measurements appeared to be insensitive to variations in grain size. This suggests that creep was primarily an intracrystalline phenomenon, and that grain boundary characteristics were unimportant. The influence of water, which appears to be quite mobile in Salado salt, was also not considered because none was ever identified in the domal salts of this study.

A comparison of the Bryan Mound creep rates in Tables B2-B8 and Table D2 shows good agreement to within the considerable scatter of the data. This means automatically that the predicted creep rates using the power-law creep parameters of Table 1, files BM3C and BM4C, are essentially the same as the predicted creep rates of earlier design analyses. In these analyses a power-law stress exponent n = 3.62 was used together with an estimated effective activation energy of Q = 12.1 kcal/mole and C = 3.16 x 10^9 s^{-1}. Note that the constant C was obtained by matching the measured estimates of steady state creep for each stress. The low value of n is attributed to a combination of non-steady state creep rates, scatter, and a very small data base. The low value of n was compensated for by the small value of C.

We stated in the introduction that design calculations inevitably require extrapolations of laboratory-based constitutive models to long times and stresses well below the stresses of laboratory tests. Long-time extrapolations require correct measurements of the rates of steady state creep. The validity of predictions at low stress must be evaluated separately, for example, in case studies of (1) salt flow around old mine workings, (2) pressure changes in SPR caverns, or (3) changes in brine levels in deep boreholes. Alternatively, efforts were made in this study to select the most applicable creep law from considerations of the physical processes governing the low-stress, low-temperature creep of rock salt. Based on comparisons of the standard errors for the fits in Tables 1 and 2, there is no doubt that power laws continue to give good descriptions of all of the existing data.

Good subgrain development in laboratory samples before laboratory testing, especially in West Hackberry salt, also indicates that dislocation climb contributed to salt creep and recovery over geologic times scales. However, there are at least four observations suggest that the power-law fits are not only due to a diffusion mechanism. (1) The effective activation energies that result from overall data fits (Table 1) and from pairs of strain rates (Table 3) remain well below the activation energy of dislocation-core-assisted volume diffusion of chlorine $Q_{SD} \approx 35$ kcal/mole. This fact is consistent with a very large standard error in Table 1 when the power-law fit for Salado salt WIPP7, the largest high-quality data set, is constrained to Q = 35 kcal/mole. (2) Activation areas that were determined at approximately constant microstructure from creep rates right before and

after changes in stress, are mostly around $100b^2$, where b is the Burgers vector for-sodium chloride (Table 3). These values lie well above $A \approx b^2$ for climb-controlled creep. (3) If power-law stress exponents are computed from pairs of estimates of steady state creep for individual samples, it becomes evident that n-values around or below five are always associated with the upper bound estimates of steady state creep of otherwise well-controlled experiments. Thus, the poorest upper bound values of $\dot{e}_{1e}$ in Table B7, stages (1b,2) give the lowest n = 2.68. In contrast, several more credible combinations of estimates of steady state creep $\dot{e}_{1e}$, exist that yield n-values above seven as shown in Table 3. Even if some of these values might be on the high side, for example, n = 7.65 for West Hackberry test QD12AN, stages (4,5), they still lie above five. This cannot be reconciled with pure climb-controlled creep. Very similar observations were made by Blum [51] in analyses for single and polycrystalline halite between 150° and 650°C. According to Blum, $n = 4.5$ when creep is climb-controlled, and $n > 5$ for stresses exceeding 300 psi. (4) Although substructural observations under this study are quite limited, it is important that the substructure of West Hackberry sample QD11AN contained no subgrains. Instead, it showed ample evidence of glide and, in our interpretation, wavy slip. These observations are especially significant because the sample had been deformed over nine percent strain which should be enough for developing an equilibrium substructure [25,27,51]. Because little strain was accumulated during recovery following four stress drops, it is reasonable to assume that the substructures shown in Figure 11 are largely representative of the substructure in this sample at the highest stress, τ = 3010 psi. Note that measurements at this stress lie well within the regime of present and earlier power-law fits.

If the conventional interpretation of power-law fits of the low-temperature creep of rock salt is ambiguous, then the question arises as to which physical processes and fits are in fact valid at and below the stresses of this study. This concern prompted the evaluation of several alternative fits, Eqs (5) and (6) in Table 2, assuming first that creep was dominated by a single mechanism. Cross-slip was the prime candidate because of several characteristics of the data, including good linear correlations of the logarithm of the estimates of steady state creep, $\dot{e}_{1e}$, on one hand, and $\log \tau$ as well as $\frac{1}{T}$ on the other. A parallel study of Salado and Asse salt also indicated that Q and n were moderately stress and temperature-dependent as required by Eq (5) [8]. Indeed, the fits for cross-slip in Table 3 provide the best descriptions with the lowest standard errors, especially for the data sets WIPP7 and BM4C that contained the least scatter. Most important, at least two of the three fitting parameters agree with corresponding values that were measured independently on single crystals. The magnitudes of B_2 in Eq (5) are equal to the activation energy for cross-slip, Q_{CS} = 3.69 ± 0.7 kcal/mole [41]; the values of In B_1 lead to reasonable preexponential terms B_1 on the order of $6.6(\pm 3) \times 10^3$ s^{-1} as reported by Skrotzki [41]. Other supportive evidence for cross-slip includes its association with wavy slip (Fig. 15c), and activation areas around $100b^2$, Eq (7) and Table 3 [8,35,37,41,52,56]. To prove the dominance of cross-slip in this study, however, it remains to be demonstrated that impurities can raise the ratio (τ_0/μ_0) for polycrystalline salt at absolute zero, Eq (5), several orders of magnitude. This value stems from the comparison of the fitting parameters $B_3 = \ln(\tau_0/\mu_0)$ in Table 2 with the value $\ln(\tau_0/\mu_0)$ = -5.43 for pure single-crystal sodium chloride [41]. It also appears necessary to collect data over a wider range

of stresses in order to verify the temperature and stress dependency according to Eq (5) by documenting the temperature and stress dependencies of Q and n in Eqs (7). Such correlations were sought by means of the data set BM4C in Figure 8b, but proved inconclusive because of difficulties in obtaining an adequate number of well-defined rates of steady state creep.

If it can be shown definitively that cross-slip is the rate-controlling process of the low-temperature, low-stress creep of rock salt throughout, then a mechanistic rationale would be available to extrapolate creep models that are based on laboratory measurements beyond the conditions of actual laboratory experiments. This could be done either with the parameters for Eq (5) in Table 3 or with the power-law models of Table 2 as good empirical approximations for cross-slip. The continued use of the power laws would be advantageous because they are already part of many structural codes.

Because of the mechanistic uncertainty related to the power law fits of Tables 1 and 3 and because of well-developed glide bands in sample QD12AN, Figure 12, it was reasonable also to test the applicability of an exponential stress model, Eq (7). In addition, variations of this expression correspond to a new, empirical glide model and to models for dislocation intersections which is an important mechanism for low-temperature creep in pure metals [35,40]. Surprisingly, the standard errors for several of these fits, Table 2, were nearly as good as the standard errors for cross-slip and for the power law. In part, this result is attributed to statistical problems that arise with small data sets, as discussed previously. However, good alternate fits were also obtained for the larger data sets BM3C, WIPP7, and WIPP4C. This underscores the difficulties of creep modeling at low stresses and temperatures when the creep rates are extremely low and considerable scatter appears inevitable. In such cases, careful consideration must be given to the mechanistic significance of the various creep parameters. Thus, on one hand, the measured values for $Q_{CS} = B_2$ in Eq (5) and Table 2 suggest cross-slip. On the other hand, low activation volumes, V, including increasing values of V with temperature, weaken the correlation with the generalized glide model, Eq (6). No ready solution is offered to improve the credibility of any particular fit. Modeling would be facilitated if measurements were available over a wider range of stresses and temperatures, but this involves the risk of crossing mechanism boundaries by going to higher stresses and substantially higher temperatures. In turn, tests at lower stresses quickly risk becoming meaningless because steady state creep is too slow to be measured, or it may never be reached, even in very long tests.

All the modeling discussed above assumed that only one process was rate-controlling throughout, including earlier Salado data in File WIPP4C, Tables 1 and 2. Based on the quality of the fits presented, this approach appeared justified. Considering the well-developed substructures in undeformed salt and reports of good subgrain development in deformed samples [27], however, it was plausible also to evaluate a two-mechanism model of cross-slip and dislocation climb. Corresponding fits were applied to the three largest available data sets, Salado salt WIPP4C and WIPP7, and Bryan Mound salt BM3C. While this effort continues, no acceptable fit has been obtained to date even if the activation energies, Q_{CS} and Q_{SD}, are prescribed and held constant. Every fit in this group had an associated standard error of the logarithm of strain rate, SE> 2.0.

It was suggested earlier that the creep under conditions of decreasing stresses is of interest to test the uniqueness of candidate steady state creep models and to assess the effects of very slow transients on design calculations. Unfortunately, neither question could be resolved in this study. The following was expected. **(1)** Complete creep recovery would occur if stress drops were followed by inverse transients to indicate substructural softening. (2) The magnitude of the inverse transients during recovery would be about the same as the transient strains after stress increments of the same magnitudes. (3) As a complicating factor, it was deemed possible that the recovery could take place in distinct stages because of known differences in the time constants for the substructural features of the different recovery processes, e.g., decreases in the dislocation density and subgrain coarsening. Our expectations were especially based on recovery observations on lithium fluoride in the dislocation climb regime and on recovery measurements on single and polycrystalline sodium chloride [51,56]. The latter measurements were made at relatively high temperatures (T> 150°C), but in a range of similar power law stress exponents, $n \geq 5.0$.

All the stress drop tests on the domal salts in Appendix B and on Salado salt in Figure 12 did show unambiguous evidence of recovery that was not recognized in the earliest tests on Salado salt in Figure 10 [10]. The occurrence of recovery was particularly well defined for West Hackberry test QD12AN, stage 4, and for the Salado test in Figure 10, stage 3. In addition, it is likely that the recovery was incomplete following the stress drops in tests **QDllAN** and QG4N (Tables B1 and B9), either because of very little creep at the reduced stresses or because of the existence of an inverse transient following an increase in temperature. However, beyond qualitative observations, the evidence does not prove or disprove the uniqueness of the steady state rates. Nor is there enough evidence to derive the governing parameters for creep recovery, including the magnitudes of the recovery strains and the durations of the recovery periods.

It is reasonable that the recovery during stages 4-6 of West Hackberry test QDllAN was incomplete compared to stage 4 of test QD12AN because, as stated before, QDllAN had been hardened more, i.e., strained more at the highest stress. Therefore, the initial creep rate, $\dot{e}_{1b}$, after the staged stress reduction for QD12AN and the subsequent creep acceleration at τ = 2430 psi was higher than the corresponding creep rate and creep acceleration for QDllAN. Thus, QD12AN moved through the required recovery strain in less time than QDllAN. It was not necessarily disturbing that the creep curve during stage 2 of QDllAN looked straight for a good bit of time (strain). Consistent with earlier remarks, this fact could merely be taken to signal the end of one recovery stage before the beginning of a second, slower stage.

Unfortunately, the reasoning applied to West Hackberry salt could not yet be verified, although the tests for salt from Bayou Choctaw, Table B9 were designed to accomplish this. For unknown reasons, the recovery of this sample during stages 9,11, and 13 appeared to be so much slower than in West Hackberry salt that the maximum creep rate, $\dot{e}_{1e}$, fell far short of the lowest estimate of steady state creep at the reference stress. This happened even after the first, short overload period with a strain accumulation of only 0.075%.

The measurements on Salado salt in Figure 12 do not clarify our understanding, perhaps because the data may be influenced by the peculiar history of this sample. This history included complete unloading and the removal of a 2-in.-thick slice before the remaining salt was reloaded. On one hand, complete recovery apparently took place very rapidly after the temperature was raised to 110°C. On the other hand, it is puzzling that the underlying microstructural adjustments during recovery were associated with only approximately 0.5% strain. This amount is considerably smaller than the magnitude of the transient strain for the same type of salt in loading tests between approximately the same stresses, $\tau \approx 1250$ psi and $\tau \approx 2900$ psi.

One last significant item needs further study. Based on earlier tests [2-4] it was always assumed that SPR design calculations were almost insensitive to the influence of transient creep [54]. This followed from closure analyses of an isolated drift in salt [58]. It is also intuitively clear because the available transient creep parameters $e_a = 2/3\gamma_a$ and ξ in the exponential model, Eq (2), imply that (1) transient creep, at constant stress, is limited to 7.8 days at most, and (2) the total transient creep, e_{1t} (γ_t) will not exceed 3.5% for Salado salt and 2.9% for West Hackberry salt. At the slower strain rates for SPR conditions, the total transient strains are predicted to be less than 1% and 0.5% at West Hackberry and Bryan Mound, respectively. The lower value for Bryan Mound salt is probably due to its finer, i.e., harder initial substructure. Of course, the determination of the transient creep parameters following earlier tests was influenced by the length of the tests and by the quality of the rates of steady state. It follows from this study that the true rates of steady state creep are lower than many of the the earlier estimates. This also implies that the earlier amounts of transient creep were underestimated. Although the transient creep will be site-specific, comparatively large transients are clearly evident in all of the data in Appendices B and C. For example, West Hackberry tests QD11AN in Figure C2 (Table B2), stage 1, is still in a transient regime at a total axial strain of 9.5%. If Eq (1) and the upper bound estimate of steady state creep for stage 1 in Table B2 are used, this means that the transient creep in this case is at least 6.3% or 2.2 times greater than transient strain that follows from earlier data fits [3]. The equivalent discrepancy for Bryan Mound salt, test QF22AN, exceeds a factor of six. The existence of relatively large transient strains must be considered in identifying equilibrium substructures corresponding to steady state conditions. They may also be important in design validation studies where design predictions are compared with in *situ* measurements made over limited periods after changes in SPR cavern pressures or wells, for example. At present, the actual *in* situ pressure changes are underpredicted by factors between 2.5 and 5 in caverns and by factors up to 10 in wells.

8 Summary and Conclusions

New creep measurements were presented for rock salt from West Hackberry and Bayou Choctaw, Louisiana, and from Bryan Mound, Texas. The measurements furnished credible upper and lower bounds of steady state creep. The upper and lower bounds

were distinguished by the association of creep with normal and inverse transients. This new approach to determining rates of steady state creep requires shorter test times than conventional methods, Possible errors in measurements of steady state creep using the new and old approaches were demonstrated by comparing two relatively large data sets for bedded salt from the Salado formation in New Mexico.

Within the scatter of data, the present measurements for West Hackberry and Bryan Mound salt agree with earlier data at 60°C. However, earlier estimates of steady state creep at 23°C were high by up to one order of magnitude because of extended transient creep.

It was verified that some of the salt from the dome at Bryan Mound creeps considerably less than West Hackberry salt. At the same time, the creep properties of Bryan Mound salt exhibited unusually large variations which led to considerable scatter in measurements. In addition, the creep properties of Bryan Mound salt from one drillhole appeared to be close to the creep properties of West Hackberry salt. The reasons for the low creep rates in Bryan Mound salt remain unknown. Chemical studies are still inconclusive; arguments about variations in initial subgrain sizes proved inadequate.

Creep measurements on Bayou Choctaw salt were limited to only one sample. Based on these limited results, the creep properties of this salt are more similar to most Bryan Mound salt than to West Hackberry salt.

The different groups of estimates of steady state creep rates in this study were fitted by a power-law creep model and by several alternate models for cross-slip, dislocation glide, and dislocation intersections. The best and mechanistically most credible fit in this group was obtained for cross-slip with excellent agreement between the fitted activation energies and activation energies for cross-slip in the literature. This conclusion is supported by activation analyses including some correlations beween the effective activation energy and the stress exponent of the power-law model (on one hand) and stress and temperature, on the other. This conclusion is also consistent with some large power-law stress exponents and with limited substructural observations that showed no subgrain development. No satisfactory fit could be obtained for a two-mechanism model for dislocation climb and cross-slip, especially when the activation energies were constrained to known values. If cross-slip can be proven to be the dominant creep mechanism, then a rationale would be available to extrapolate the existing measurements of steady state creep beyond the range of laboratory conditions of stress and temperature. Such extrapolations appear justified also by equivalent salt viscosities [39] of the order of 10^{19} poise or less that are predicted by the cross-slip model for geologic stresses, $100 \leq \tau \leq 250$ psi and corresponding temperatures $70" \leq T \leq 120°C$.

Although the present data suggest that cross-slip may be the rate controlling step during the low-temperature creep of this study, there is good agreement between the cross-slip and power-law fits. Therefore, the power-law fits appear to be good empirical approximations to the true creep processes despite the fact that the fitted power-law creep parameters *cannot be interpreted* mechanistically.

Creep measurements after stress drops showed that recovery occurred, as evidenced

by the development of inverse transients with attendant creep acceleration. However, in some cases, the recovery proceeded so slowly that it was recognized only after it was accelerated by increases in temperature. At the least, this means that the time constants for transient creep after stress reductions differ from the time constants following stress increases. However, it remains to be proved that complete recovery will occur under all circumstances, especially if only one recovery process such as cross-slip is active. To accomplish this, ongoing substructural measurements will have to be completed on deformed salt before and after stress drops. In addition, recovery will have to be carried out to larger recovery strains than were accumulated in this study.

Comparisons of transient creep strains collected here and in earlier tests indicate that transient creep lasts longer than is predicted by an exponential transient creep model derived from creep data for Salado salt. The present results also suggest that the transient creep strains are larger than predicted. Both of these observations should be considered in validation studies with comparisons of predicted salt motions and deformations that are monitored *in situ*.

9 References

1. Herrmann, W., Wawersfk, W.R., and Lauson, H.S.
   Analysis of Steady State Creep of Southeastern New Mexico Bedded Salt, SAND80-0558, Sandia National Laboratories, 1980.
2. Herrmann, W., Wawersfk, W.R. and Lauson, H.S.
   A Model for *Transient Creep* of Southeastern New Mexico *Salt*, SAND80-2172, Sandia National Laboratories, 1980.
3. Wawerstk, W.R., Hannum, D.W., and Lauson, H.S.
   Compression and Extension Data for Dome Salt from West Hackberry, Louisiana SAND79 0668, Sandia National Laboratories, 1979.
4. Wawerslk, W.R., Holcomb, D.J., Hannum, D.W., and Lauson, H.S.
   Quasi-Static and *Creep* Data for Dome Salt from Bryan Mound, Texas SAND80-1434, Sandia National Laboratories, 1980.
6. Hansen, F.D. and Carter, N.L.
   Creep of Avery Island Rock Salt, Proc. 1" Conf. Mech. Behavior of Salt, Penn. State Univ., 1981 (in press).
6. Herrmann, W. and Lauson, H.S.
   Analysis of Creep Data *for* Various Natural Rock Salts, SAND81-2567, Sandia National Laboratories, 1981.
7. Albrecht, H. and Hunsche, U.
   Gebirgsmechanische *Aspekte bei* der *Endlagerung* radioaktiver *Abfälle* in Salzdiapiren unter *besonderer Beriicksichtigung des* Fliessverhaltens von Steinsalz, Fortschr. Miner.,58, 212-247, 1980.
8. Wawerslk, W.R.
   Determination of Steady State *Creep* Rates and Activation Parameters for Rock Salt. High *Pressure, High Temperature Testing of Rock,* Special Technical Publication of ASTM (in press).
9. Hansen, F. D.
   Quasi-Static *and Creep* Deformation Characteristics *of Bedded* Salt *from* the Carey Mine Near *Lyons,* Kansas, Report RSI-0067, RE/SPEC, Inc., 1978.
10. Wawerstk, W.R. and Hannum, D.W.
    Interim Summary of Sandia *Creep* Experiments *from the WIPP Study* Area, Southeastern New Mexico, SAND790115, Sandia National Laboratories, 1979.
11. Herrmann, W., Wawerslk, W.R., and Lauson, H.S.
    Creep Curves and Fitting Parameters for Southeastern New Mexico Bedded Salt, SAND80-0087, Sandia National Laboratories, 1980.
12. Wawersik, W.R. and Preece, D.S.
    Creep Testing of Salt- Procedures, Problems and Suggestions, Proc. 1" Conf. Mech. Behavior of Salt, Penn. State Univ., 1981 (in press).

13. **Weertman, J.**
Dislocation *Climb* Theory of Steady State Creep, Am. Soc. Met.. Trans. Quart. 61, 681-694, 1968.

14. **Whitlng, G.H., Woodward-Clyde Consultants, and Beasley, R.R.**
SPR Geological Site Characterization Report West Hackberry ***Dome,*** SAND80-7131, Sandia National Laboratories, **1980.**

16. **Tillerson, J.R., D'Appolonia Consulting Engineers, Inc., and Beasley, R.R.**
SPR* Geological *Site* Characterization *Report Bryan ***Mound Dome,*** SAND80-7111, Sandia National Laboratories, 1980.

16. **Hogan, R.G, Gubbels, M.H., Acres American, Inc., and Beasley, R.R.**
Strategic Petroleum *Reserve (SPR)* Geological Site Characterization Report *Bayou Choctaw* Salt *Dome,* SAND80-7140, Sandia National Laboratories, 1980.

17. **Bild, R.W.**
Chemistry and *Mineralogy of* Samples from the Strategic Petroleum *Reserve* Bryan *Mound Site,* SAND80-1258, **Sandia National Laboratories, 1980.**

18. **Bild, R.W.**
Chemistry *and Mineralogy* of Samples *from* the Bayou Choctaw, *Bryan* Mound, Sulfur *Mines, Weeks* Island *and West Hackberry Strategic Petroleum Reserve Sites, November 1979 through* August 1982, SAND83-0630, **Sandia National Laboratories, 1983.**

19. **Krumhansl, J.L. and Reece, M.**
Reconnaissance Analysis of Salt Samples, Memorandum, Sandia National Laboratories, July 7, **1983.**

20. **Hlava, P. and Krumhansl, J.L.**
Personal communication, Sandia National Laboratories, 1983.

21. **Gibeling, J.C.**
***The* Use of *Stress* Change *Experiments to Study the Mechanisms of* Elevated Temperature *Deformation,* Ph.D. Thesis, Stanford University, 1979.**

22. **Blum, W. and Ilschner, B.**
***Ueber das Kriechverhalten von NaCl-Einkristallen,* phys. stat. sol., 20, 1503-1530, 1967.**

23. **Pharr, G.M.**
Personal communication, **Rice University, 1981.**

24. **Robinson, S.L., Burke, P.M., and Sherby, O.D.**
Activation Energy and Subgrain Size-Creep Rate Relations in Sodium Chloride, Phil. Mag., **29**,423-427, **1974.**

26. **Eggeler, G. and Blum, W.**
***Coarsening of* the *Dislocation Structure After Stress Reduction During Creep of NaCl Single* Crystals, Phil. Mag. A, 44,, 5, 1065-1084, 1981.**

26. **Ferreira, I.**
The Effect of Stress Reductions During* the Steady State *Creep in High Purity Aluminum, PhD **Thesis, University of Washington, 1978.**

27. **Carter, N.L. and Hansen, F.D.**
***Creep of* Rocksalt, Tectonophysics, 92, 275-333, 1983.**

28. **Sherby, O.D. and Burke, P.M.**
Mechanical *Behavior* of Crystalline Solids at Elevated *Temperature, Prog. Mat.Sci.*, 13, 322-390, 1968.

29. Jefferson, T.H.
TJMAR1-A FORTRAN Subroutine for Nonlinear Least Squares Parameter Estimation, SLL73-0305, Sandia National Laboratories, 1973.

30. Barr, L.W., Hoodless, J.A., Morrfson, I.M., and Rudham, R.
Effects of Gross Imperfections on Chloride Ion Diffusion in Crystals of Sodium Chloride and Potassium Chloride, Trans. Faraday Soc., 56, 697-708, 1960.

31. Draper, N.R. and Smtth., H.
Applied Regression Analysis, John Wiley&Sons, Inc., 1981.

32. Pfeifle, T.W. and Senseny, P.E.
Steady-State Creep of Rock Salt in Geoengineering, Proc. 23rd U.S. Symp. Rock Mech., Univ. Calif. Berkeley, 1982.

33. Burke, P.M.
High Temperature Creep of Polycrystaline Sodium Chloride, Ph.D. Thesis, Stanford University, 1968.

34. Seeger, A., Berner, R., and Wolf, H.
Die experimentelle Bestimmung von Stapeifehlerenergien *kubisch-flächenzentrierter* Metalle, Z. Phys., 156, 247, 1959.

35. Conrad, H.
The Experimental Evaluation of *Creep* and Stress Rupture, In *Mechanical Behavior of Materials at Elevated Temperatures,* J. E. Dorn, ed., McGraw Hill, 149-217, 1961.

36. Schoeck, G.
The Activation Energy of Dislocation Movement, phys. stat. sol., 8, 499,507, 1965.

37. Evans, A.G. and Rawlfngs, R.D.
The Thermally Activated Deformation of Crystalline Materials, phys. stat. sol., 34, Q-31, 1969.

38. Kocks, U.F., Argon, A.S., and Ashby, M.F.
Thermodynamcia and Kinetics of Slip, Prog. Mat. Sci., 4, Pergamon Press, 1975.

39. Heard, H.C.
Steady State Flow *of Polycrystalline* Halite at *Pressure of 2* Kilobars, *Flow and Fracture of Rocks,* Am. Geophys. Union, Monograph 16, 191-209, 1972.

40. Nix, W.D. and Ilschner, B.
Mechanisms Controlling Creep of Single Phase Metals *and Alloys,* Proc. 5th Int. Conf. on the Strength of Metals and Alloys, Aachen, 1979, Pergamon Press, 1980.

41. Skrotzki, W. and Liu, Z.G.
Analysis of the Cross Slip Process in Alkali Halides, phys. stat. sol., 73, K225-K229, 1982.

42. Ahlquist, C. N. and Nix, W. D.
The Measurement of Internal *Stressses* During *Creep* of *Al* and Al-Mg Alloys, Acta Metall., 19, 373-385, 1971.

43. Blum, W.
On Modelling Steady State and Transient Deformation *at* Elevated *Temperature,* Scripta Met., 16, 1353-1357, 1982.

44. Jones, W.B. and Rohde, R.W.
Measuring Back Stresses in Commercial *Alloys* at Elevated Temperature, *Novel Techniques* in *Metal Deformation* Teating, R. H. Wagoner, ed., Met. Soc. AIME. 373-389, 1983.

45. **Wawersik, W.R.**
Unpublished Data, Sandia National Laboratories, 1984.

46. **Gibbs, G.B.**
Creep and Stress Relaxation Studies *with Polycrystalline* **Magnesium, Phil. Mag., 317-329, 1965.**

47. **Woodford, D.A.**
Measurement and Interpretation of the *Stress* **Dependency of Creep at Low Stress, J. Mat. Sci. Engr., 4, 146154, 1969.**

48. **Pontikis, J.P. and Poirier, J.P.**
Phenomenological and Structural Analysis of Recovery-Controlled *Creep with Special Reference* **to** *the Creep* **of** *Single* **Crystal** *Silver* **Chloride, Phil. Mag., 32, 3, 577-592, 1975.**

49. **Pontikis, J.P.**
Phenomenological Analysis of Recovery Controlled *Transient Creep* **Supported by Substructural Observations in** *Single* **Crystal Sodium Chloride and** *Silver* **Chloride,** Acta Metall., **26, 847-855, 1977.**

50. **Gupta, V.P. and Strutt, P.R.**
Dislocation Structures in Copper Single Crystals Deformed in High Temperature *Creep,* **Can. J. Phys., 46, 1213-1220, 1967.**

61. **Blum, W.**
Activation *Analysis of the* **Steady-State Deformation of Single- and Polycrystalline Sodium Chloride, Phil. Mag., 28, 245-259, 1973.**

62. **Blum, W.**
Stationäre **Verformung von polykristallinem Natriumchlorid,** Ph.D. Thesis, Universität Erlangen-Niirnberg, FRG, **1969.**

53. **Lsngdon, T.G., Vastavs, R.B., and Yavari, P.**
The **Influence of Substructure on Creep Behavior Following** *Stress* **Changes,** Proc. 5^{th} **Int. Conf. on the Strength of Metals and Alloys, Aachen, 1979, Pergamon Press, 271-276, 1980.**

64. **Murty, K.L. and McDonald, S.G.**
Effect of Prior *Creep* **on Steady State** *Creep* **Behavior** *of* **Stainless Steel** *Type* **304, Mat. Sci. Engr., 66, 105-109, 1982.**

66. **Preece, D.S. and Foley, J.T.**
Finite Element Analysis of Salt Caverns Employed in the Strategic Petroleum Reserve, Proc. 4^{th} **Intern. Symp. on Salt, Toronto, Canada, May 1983 (in press).**

66. **Hesse, J.**
Die Plastische Verformung von Natriumchlorid, phys. stat. sol., 9, 209-230, 1965.

67. **Streb, G. and Reppich, B.**
Steady State Deformation and *Dislocation* **Structure of Pure and Mg-Doped** *LiF* **Single Cyrstals, phys. stat.** sol., **16, 493-505, 1973.**

68. **Wawersik, W.R., Herrmsnn, W., Montgomery, S.T., and Lauson, H.S.**
Excavation Design in Rock Salt-Laboratory Measurements, Material Modeling and Validations, Proc. **Int. Symp. Rock** Mech. **Related to Caverns and Pressure Shafts, hachen, Germany, May 2628, 1982 (in press).**

Table 1. Power-Law Fitting Parameters

Origin of Salt-File	Fitting Parameters			
	C s^{-1}	n	Q cal/mole	SE
West Hackbr.—				
WH1	3.30×10^{14}	4.73	13,120	0.231
WH2	7.92×10^{12}	4.99	9,420	0.231
WH2*	1.79×10^{15}	5.06	12,750	0.221
WH4	9.35×10^{28}	13.00	13,120	1.06
WH5	2.23×10^{32}	14.25	13,120	0.371
WH1	1.94 x 10"	4.90	12,000	0.195
Bryan Mound—				
BM3C	1.61×10^{14}	4.54	15,140	0.519
BM4C	5.26×10^{18}	5.18	17,830	0.149
BM6C	2.40×10^{10}	3.54	13,460	0.719
Bayou Choctaw—				
BC1	8.45×10^{10}	4.06	11,830	0.811
Salado—				
WIPP4C	4.46×10^{14}	4.90	12,000	1.01
WIPP7	7.97×10^{17}	5.09	16,550	0.441
WIPP7	6.54×10^{47}	11.36	35,000	1.79

Legend: **WH1, BM3C, BM4C, BC1** and **WIPP7**: New creep data for stress increment tests (Appendix B and Ref. 8). **BM3C** contains all Bryan Mound data except for salt from drillhole BM113. **BM4C** contains only data for BM113.

WH2, **BM6C**: Combined old and new creep data for stress increment tests (Appendices B and Ref. 8). **BM6C** contains all Bryan Mound data except for data for salt from drillhole BM113.

WH2*: Same as WH2 but without measurements at 22°C.

WH4 and WH5: New creep data for stress drop tests (Appendix B) including and excluding datum for test QD12AN.

WIPP4C: Combined old and new creep data for stress increment test [1,11].

SE≡standard error of logarithm of fit.
Underlined values were constrained to the numbers shown.

Table 2. General Fitting Parameters

Site— File	Eq #	Fitting Parameters to Eq(#) in Column 1 and Standard Error to Logarithm of Fit							
		In B_1	B_2	B_3	B_4	B_5	B_6	B_7	SE
West Hackb.-									
WH1	5	2.14	3,320	-2.43	–	–	–	–	0.188
Bryan M.–									
BM3C	5	3.55	3,370	-1.366		–	–	–	0.517
	6	3.98	Q	18,840	1.15	Q	Q	Q	0.557
	6	65.39	9.65	11,300	-1.26	Q	Q	Q	0.542
BM4C	5	9.37	3,440	-1.345		–	–	–	0.142
	6	9.29	Q	21,270	1.30	Q	Q	Q	0.142
	6	5.80	Q	18,960	2.51	4,393	Q	Q	0.170
Bayou Ch.–									
BC1	5	-2.18	2,688	-2.34		–	–	–	0.811
	6	-2.18	Q	14,340	1.17	Q	Q	Q	0.811
Salado—									
WIPP4C	5	-1.519	3,088	-3.275		–	–	–	1.03
	6	-3.08	Q	12,540	1.189	Q	Q	Q	1.168
	6	-10.8	Q	7,800	17.0	1,623	Q	Q	1.031
WIPP7	5	5.516	3,521	-2.301		–	–	–	0.435
	6	4.39	Q	18,390	1.61	Q	Q	Q	1.168
	6	26.09	2.99	17,370	1.29	Q	0.47	Q	0.456
	6	28.10	2.98	17,780	0.68	Q	Q	0.5	0.445
	6	1.174	Q	16,160	3.95	611	Q	Q	0.452
	6	1.178	Q	16,170	9.87	610	0.6	Q	0.451

Legend: WH1, BM3C, BM4C, BC1 and WIPP7: New creep data for stress increment tests (Appendix B and Ref. 8). BM3C contains all Bryan Mound data except for salt from drillhole BM113. BM4C contains only data for BM113.

WH2, BM6C: Combined old and new creep data for stress increment tests (Appendices B and Ref. 8). BM6C contains all Bryan Mound data except for data for salt from drillhole BM113.

WH4 and WH5: New creep data for stress drop tests (Appendix B) including and excluding datum for test QD12AN.

WIPP4C: Combined old and new creep data for stress increment test [1,11].

SE≡standard error of logarithm of fit.
Underlined values were constrained to the numbers shown.

Note that the parameters B_2 and B_3 in Eqs (5) and (6) have different physical significance and dimensions. For example, B_2 in Eq (5) is the activation energy for cross-slip, Q_{CS}, in cal/mole. B_2 in Eq (6) is a dimensionless exponent of stress.

Table 3. Activation Parameters for Selected Measurements in Appendix B

Site-Test I.D. (Test Stages)	Activation and Test Parameters				
	A/b^2	A H cal/mole	n	Stresses psi	Temprs. °C
West Hackbr.—					
QD12AN					
(1,2)	–	–	4.91	1,972/2,435	60
(2,3)		15,120	–	2,418	60/80
(3,4)		24,180	–	2,426	80/60
(2,5)		–	4.99	2,435/2,925	60
(4,5)	–	–	7.65	2,457/2,925	60
QD11AN					
(1,2)	86	–	–	2,722/3,010	60
(2,3)	68	–	–	2,441/2,732	60
Bryan Mound—					
QF22AN					
(4,5)	–	18,070	–	2,888	60/100
(5,6)	–	19,070	–	2,903	100/60
QF34N					
(1,2)	64	–	–	2,064/3,150	60.3
QF35N					
(4,5)	346	–	–	2,083/2,231	59.8
(6,7)	–	14,080	–	2,214	80/59.6
(7,8)	99	–	–	2,212/2,983	59.6
(8,9)		16,020	–	2,978	59.5/80
(9,10)	–	17,050	–	2,975	80159.4
(12,13)	–	18,000	–	3,551	59.4180
(13,14)	–	15,070	–	3,546	80/33.5
QF36N					
(1b,2)	75	–	2.68	2,356/3,270	59

Table 3 cont. Activation Parameters for Selected Measurements in Appendix B

ite-Test I.D. (Test Stages)	Activation and Test Parameters				
	A/b^2	Q cal/mole	n	Stresses psi	Temprs. °C
Bryan Mound—					
QF37N					
(1,2)	–	14,280	–	2,498	40,60
(2,3)	–	18,870	–	2,487	60,80
(3,4)	–	20,460	–	2,483	80,59.8
(4,5)	–	15,560	–	2,489	59.8,39.8
(5,6)	86	–	7.88	2,490/2,848	39.9
(6,7)	–	17,400	–	2,842	40,59.8
(7,8)	–	17,800	–	2,839	59.8,40
(8,9)	–	19,280	–	2,836	40,79.6
(9,10)	–	20,960	–	2,837	79.6,59.8
(4,7)	–	–	7.19	2,488/2,836	59.8
ayou Choctaw					
QG4N					
(2,3)	106	–	–	2,135/1,857	80
(6,7)	–	20,020	–	2,136	80,60
(7,8)	174	–	–	2,139/2,475	60
(9,10)	201	–	–	2,152/2,462	60
(11,12)	198	–	–	2,159/2,471	60
(12,13)	81	–	–	2,471/2,151	60
(7,12)	–	–	8.22	2,139/2,471	60

Legend:

$A/b^2 \equiv$ activation area divided by square of Burgers vector ($b=3.99\ cm^{-8}$), Eq (12)

nrpower-law stress exponent, Eqs (3) and (7).

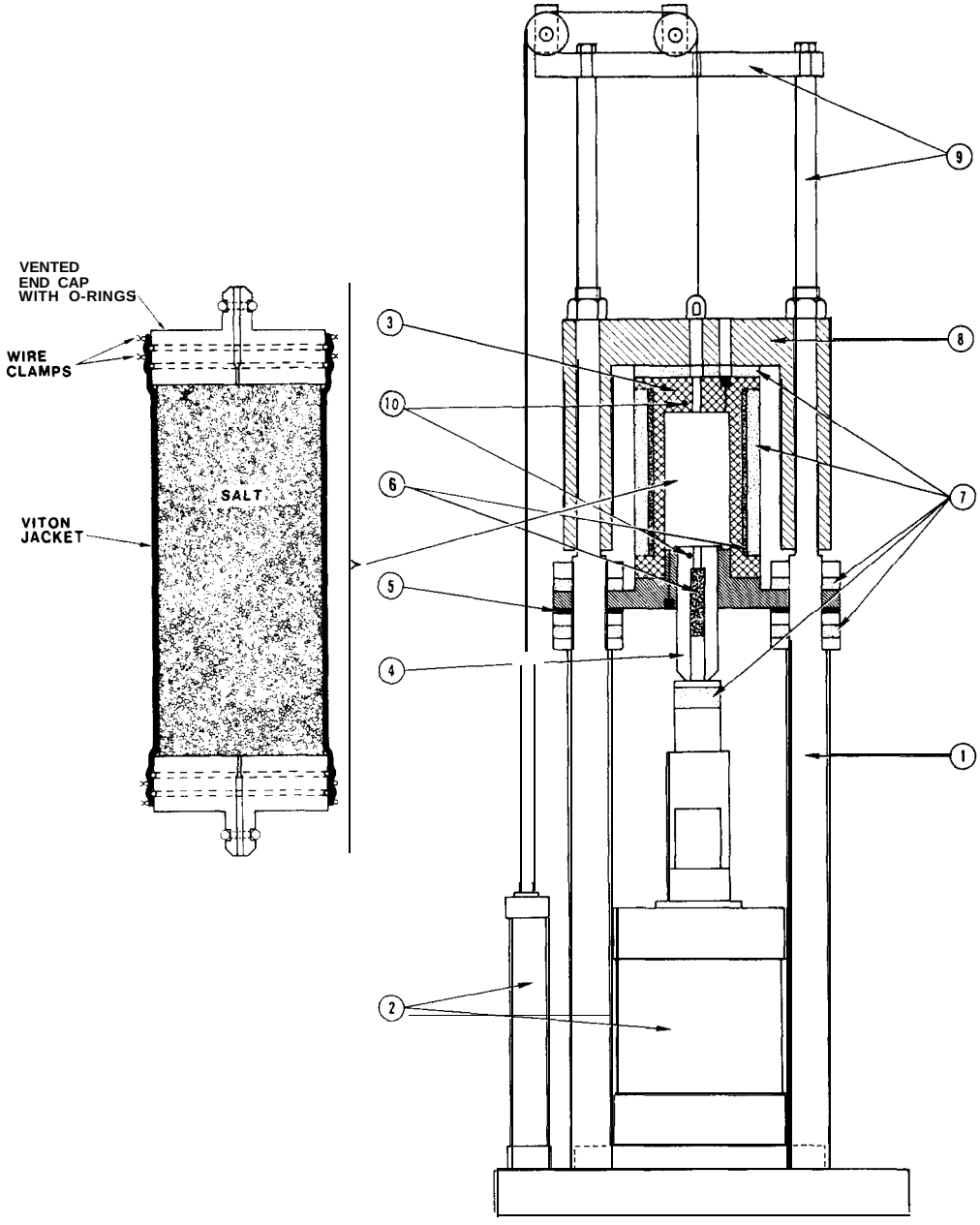

Figure 1. Schematic of creep apparatus. Major components: **(1)** tie rods on base plate, **(2)** hydraulic actuators, (3) pressure vessel, (4) deviatoric loading piston, (5) Belleville washers, (6) heaters, (7) insulation, (8) cross head with guide rods, (9) frame extension/lifting fixture, **(10)** thermocouple location.

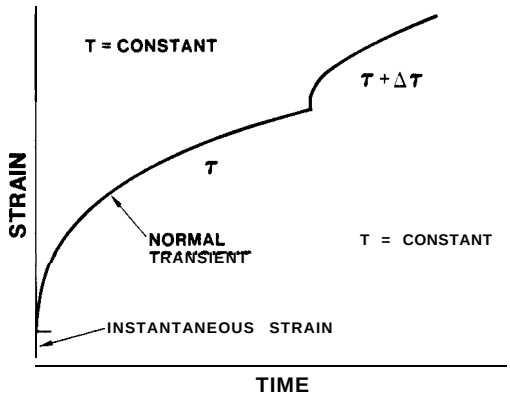

(a)

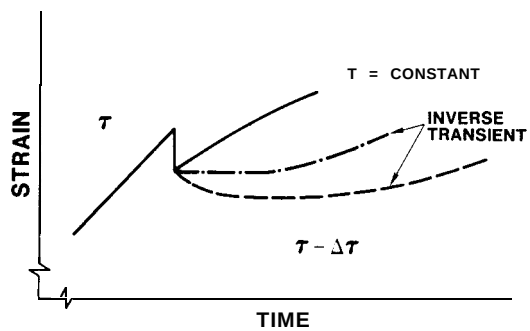

(b)

Figure 2. Schematic of transients after stress changes. (a) Normal transient after stress increase. (b) Normal and inverse transients, following stress drop.

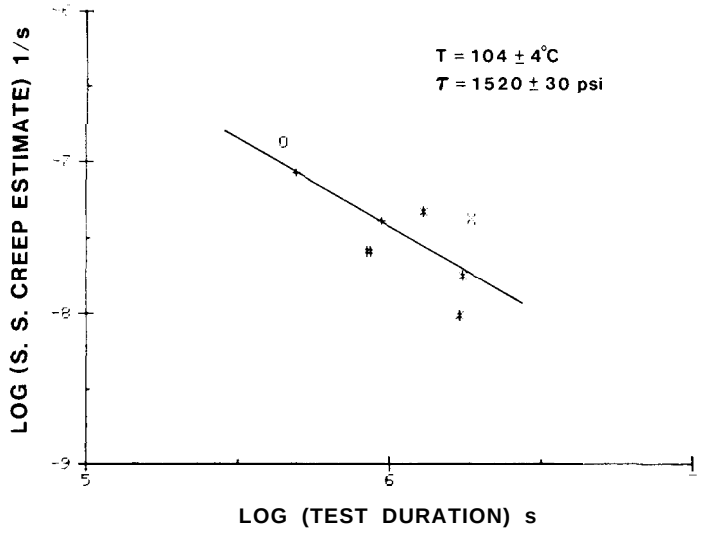

Figure 3. Correlation between estimates of steady state creep and test duration of early creep data for Salado salt [23]

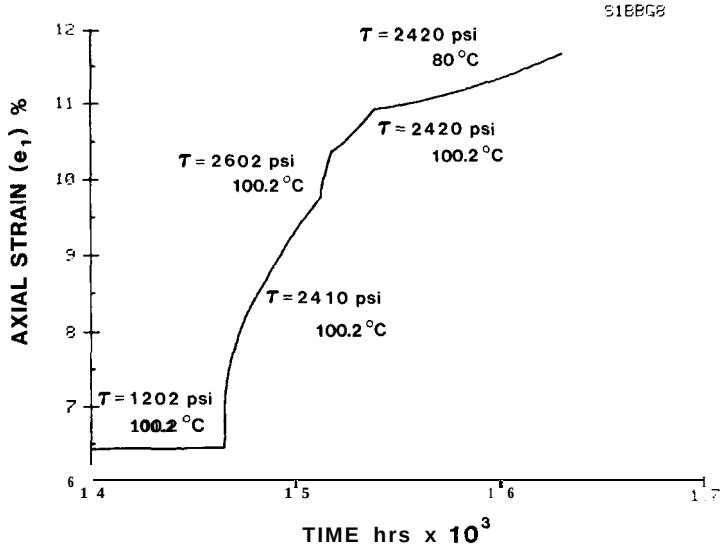

Figure 4. Creep records of stress and temperature change tests. Note transients associated with stress cycle from τ = **2410** psi to 2602 psi and back to τ = 2420 psi; $\tau = (\sigma_1 - \sigma_3) \equiv$ applied stress.

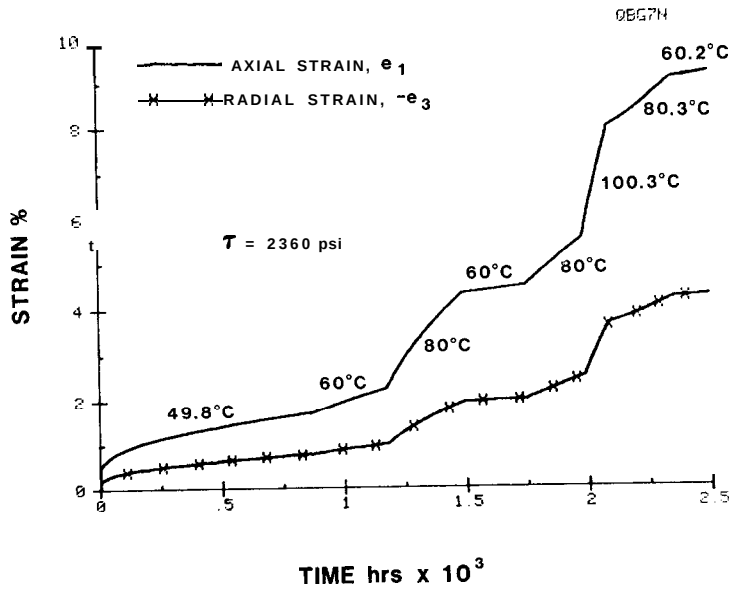

(a)

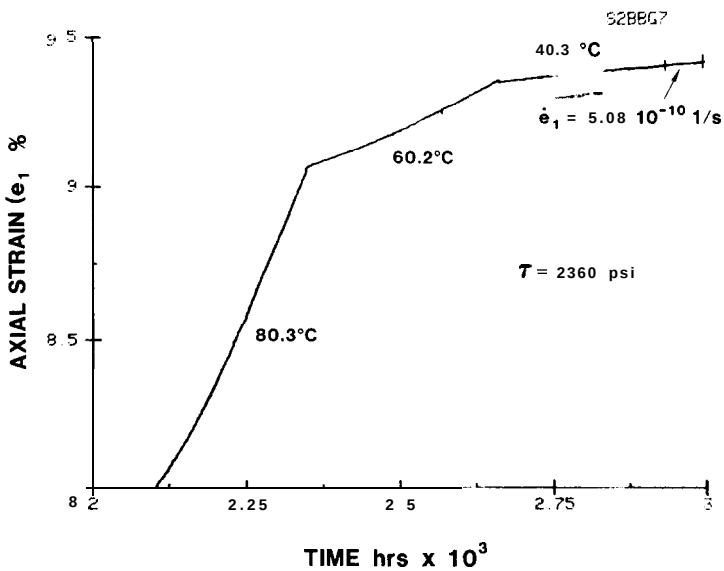

(b)

Figure 5. (a) Axial and radial strains of multistage creep test at different temperatures. (b) Inverse transients following temperature drops.

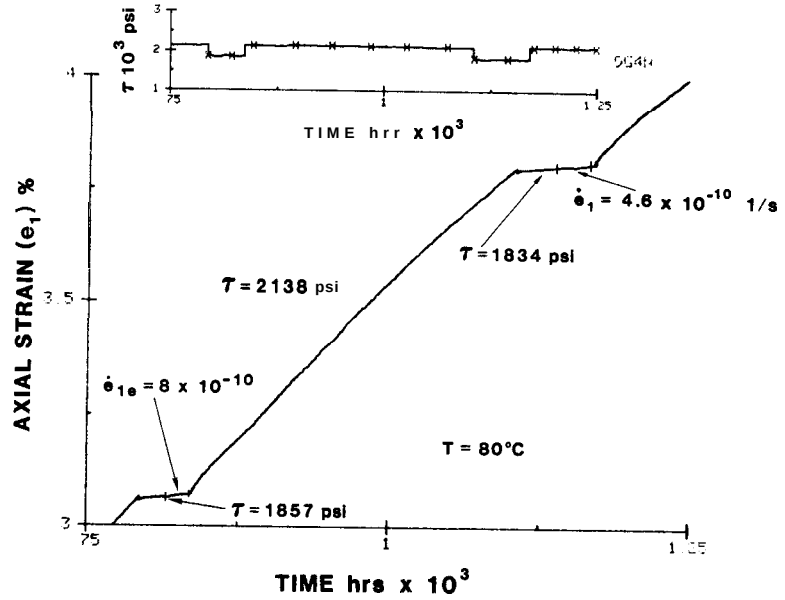

Figure 8. Record of creep experiment with intermittent, short-term stress drops. Insert shows stress history during interval in main figure.

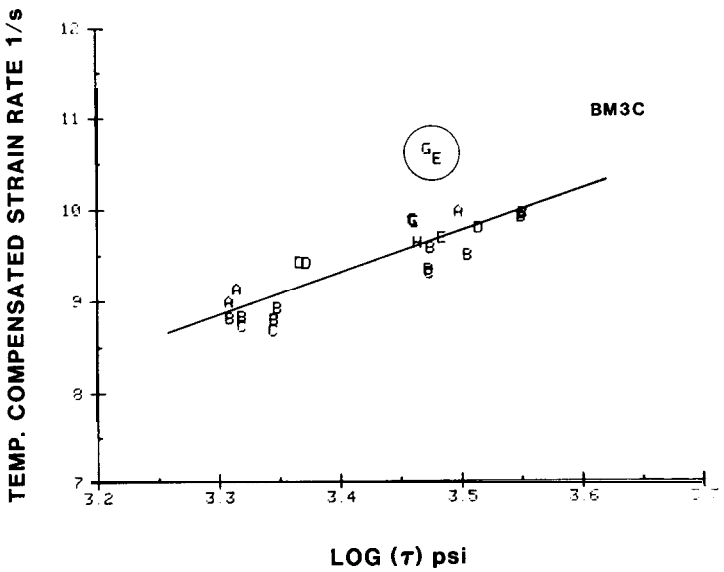

Figure 7. New temperature-compensated estimates of steady state creep, $\dot{e}_{1e}\ exp(Q/RT)$, versus applied stress, τ, for Bryan Mound salt, drillholes 107A, 107C, and 108B (Tables B3-B7). Letters identify different samples and test stages. The encircled points G and E correspond to measurements at 22°C.

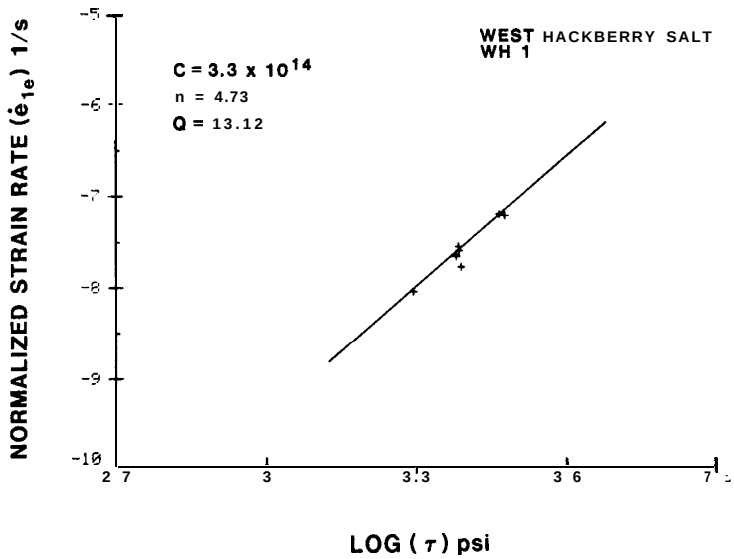

Figure 8a. Temperature-normalized estimates of steady state creep for West Hackberry salt, $\dot{e}_{1e}\ exp\big((Q/RT) - (Q/R333)\big)$, versus applied stress, τ. Normalization temperature is 60°C, Q = **13.12** kcal/mole (Table **1).**

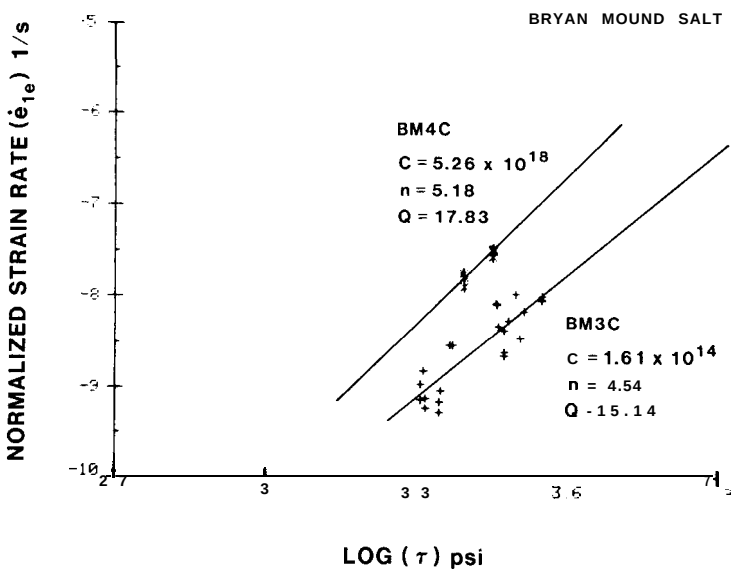

Figure 8b. Temperature-normalized estimates of steady state creep for Bryan Mound salt, $\dot{e}_{1e}\ exp\big((Q/RT) - (Q/R333)\big)$, versus applied stress, τ. Normalization temperatures is 60°C, Q = **15.14** and **17.83** kcal/mole (Table **1).** File BM3C consists of data of Tables B3-B7, without 22°C measurements in Table B3. File BM4C contains steady state creep estimates of Table B8. Note large scatter in data of BM3C.

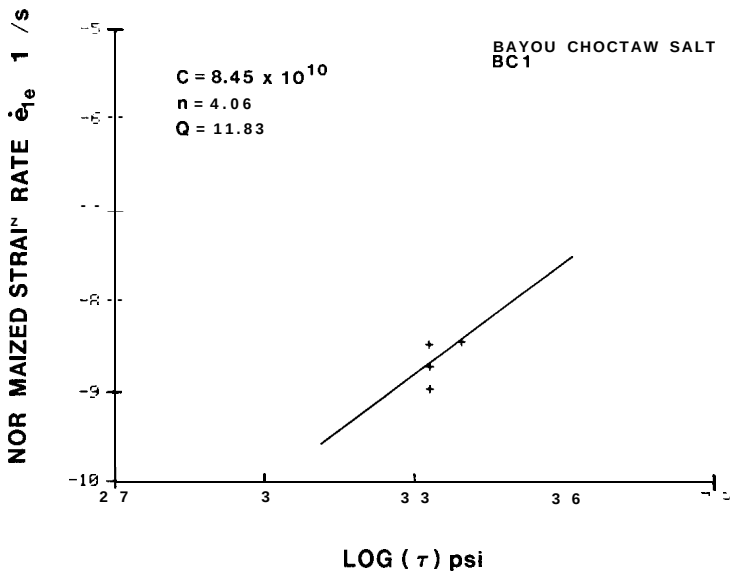

Figure 8c. Temperature-normalized estimates of steady state creep for Bayou Choctaw salt, $\dot{e}_{1e}\, exp\big((Q/RT) - (Q/R333)\big)$, versus applied stress, τ. Normalization temperature is 60°C, **Q = 11.83** kcal/mole (Table **1).**

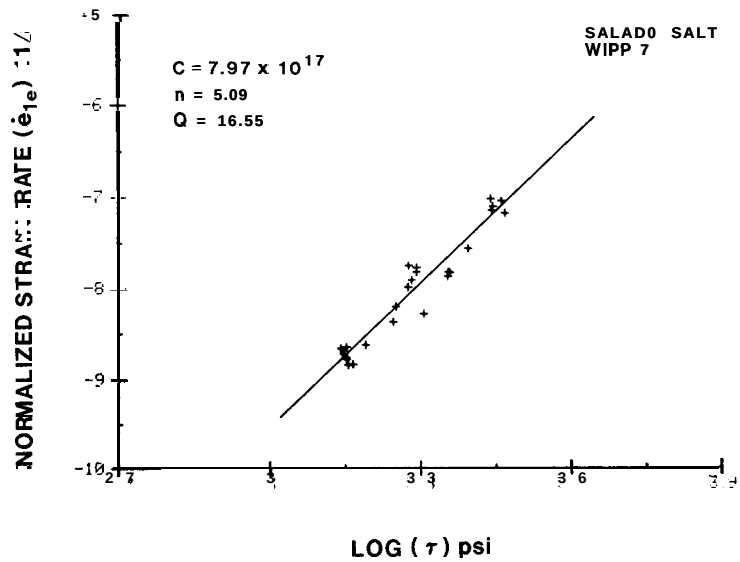

Figure 8d. Temperature-normalized estimates of steady state creep for Salado salt, $\dot{e}_{1e}\, exp\big((Q/RT) - (Q/R333)\big)$, versus applied stress, τ. Normalization temperature is 60°C, Q = 16.55 kcal/mole (Table **1,** File WIPP7).

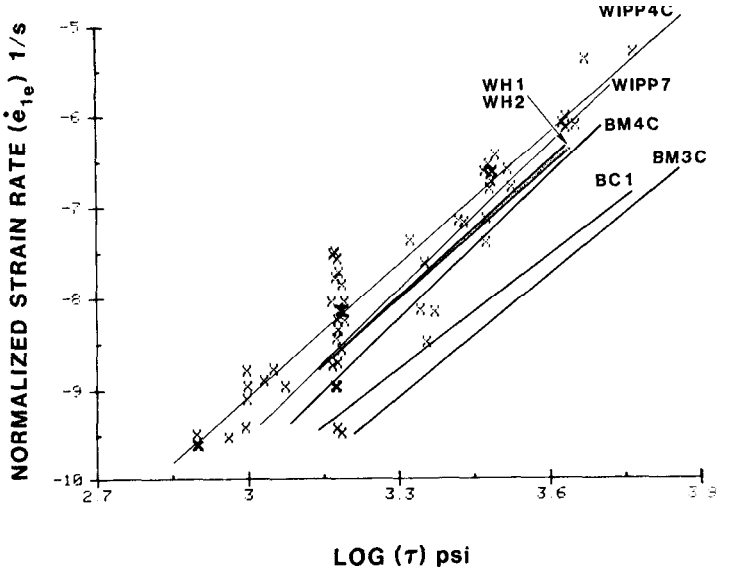

Figure 8e. Power-law fits for 60°C for West Hackberry salt (Files WH1 and WH2, Table 1), Bryan Mound salt (Files BM3C and BM4C), Bayou Choctaw salt (File BC1), and Salado salt (Files WIPP7 and WIPP4C). The data points shown are temperature-compensated, upper-bound estimates of steady state creep for Salado salt (File WIPP4C) used for reference in earlier data analyses and design calculations [3,4,55]. Model parameters used are listed in Table 1.

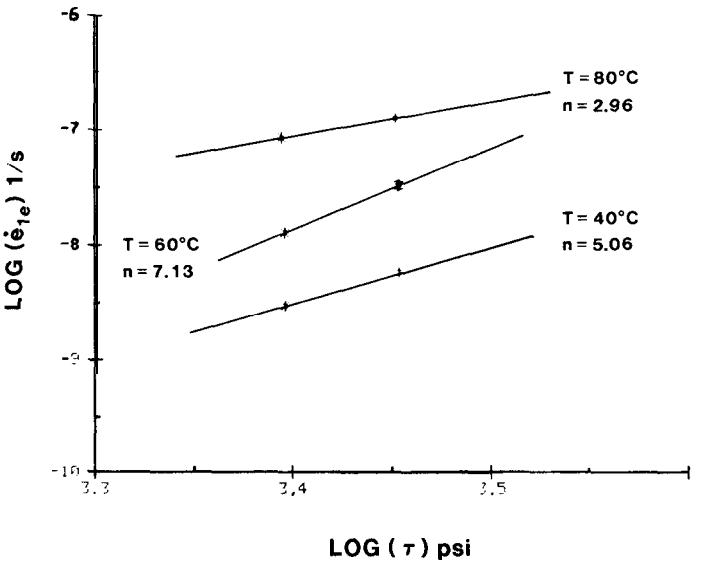

Figure 9. Power-law correlations of estimates of steady state creep, $\dot{e}_{1e}$, for Bryan Mound sample BM113-4225 (Table B8) at different temperatures.

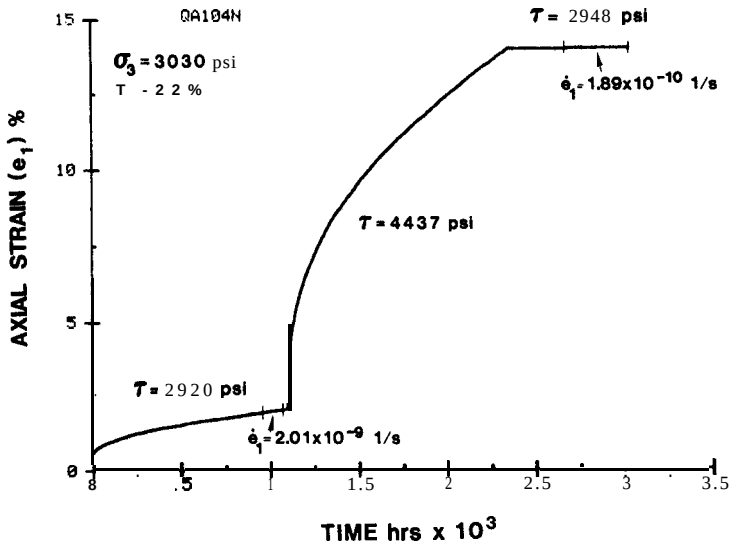

Figure 10. Creep data for Salado salt subjected to $\tau \approx$ 2900 psi before and after creep at a higher stress [10].

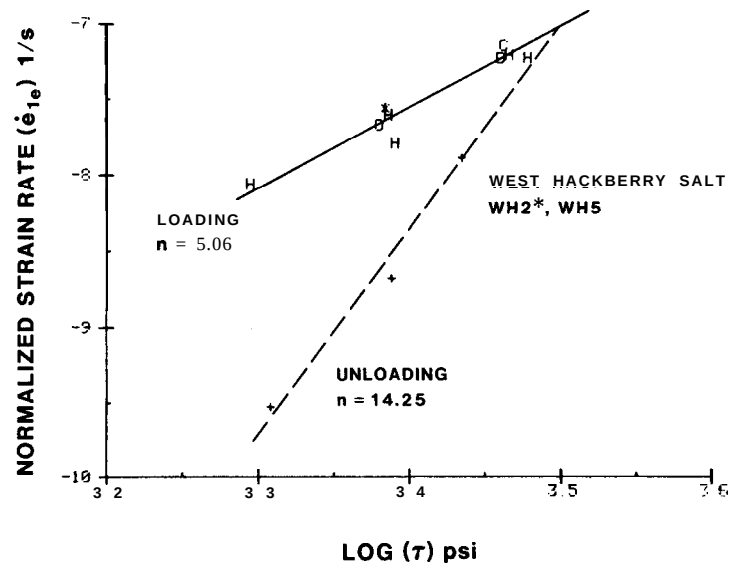

Figure 11. Comparison of estimates of steady state creep, $\dot{e}_{1e}$, measured in stress increment (loading) and stress drop (unloading) tests on West Hackberry salt (Files WH4 and WH5 in Table **1;** Tables **Bl** and B2). A,B,C,D≡loading data; *,+≡stress drop measurements.

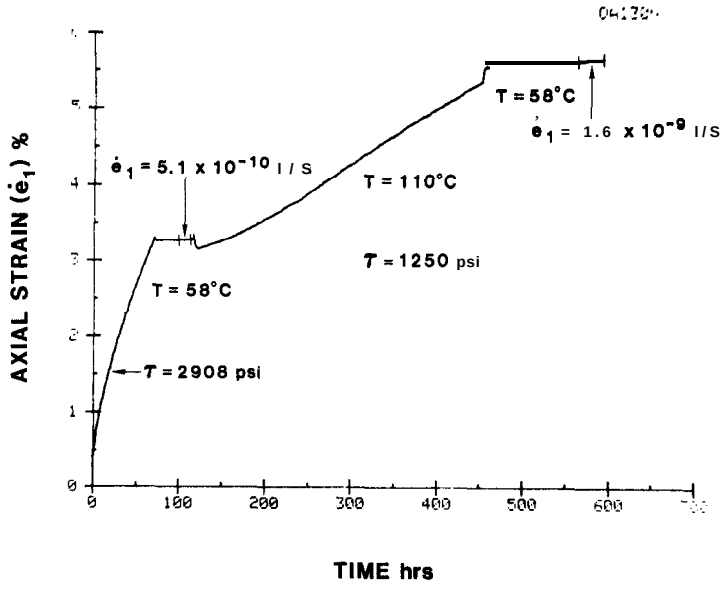

Figure 12. Recovery measurements on Salado salt following stress drop and temperature change.

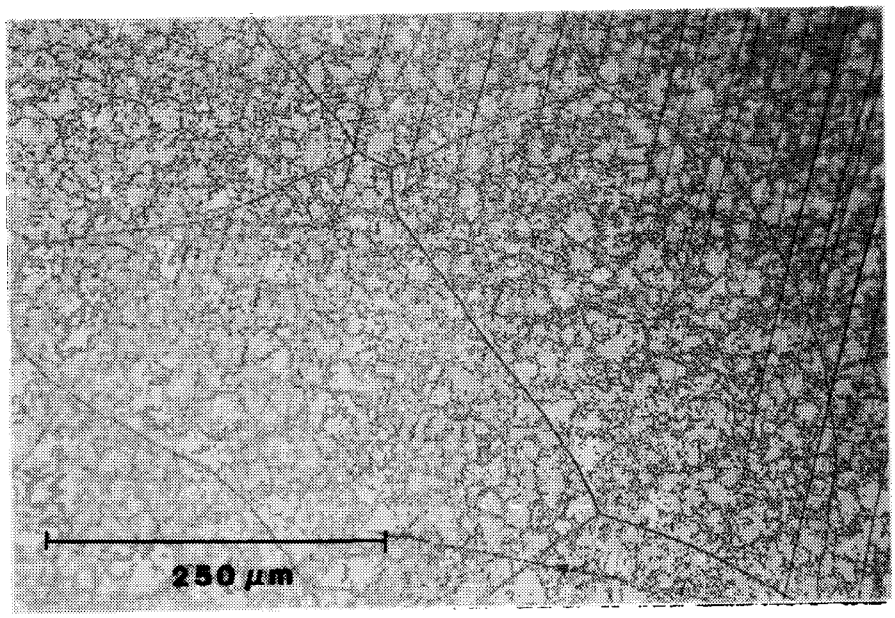

Figure 13. Initial substructure of West Hackberry salt, sample WH108-2293. Individual dots are individual etch pits, i.e., intersections of dislocation lines with sample surface. Dark lines are subgrain boundaries consisting of dense dislocation arrays.

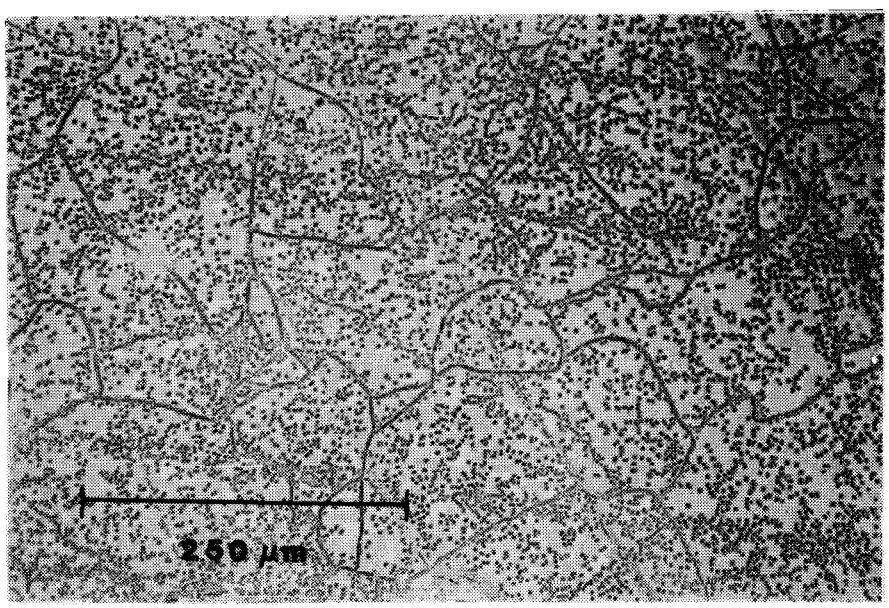

Figure 14. Initial substructure of Bryan Mound salt, sample BM107B-2205.

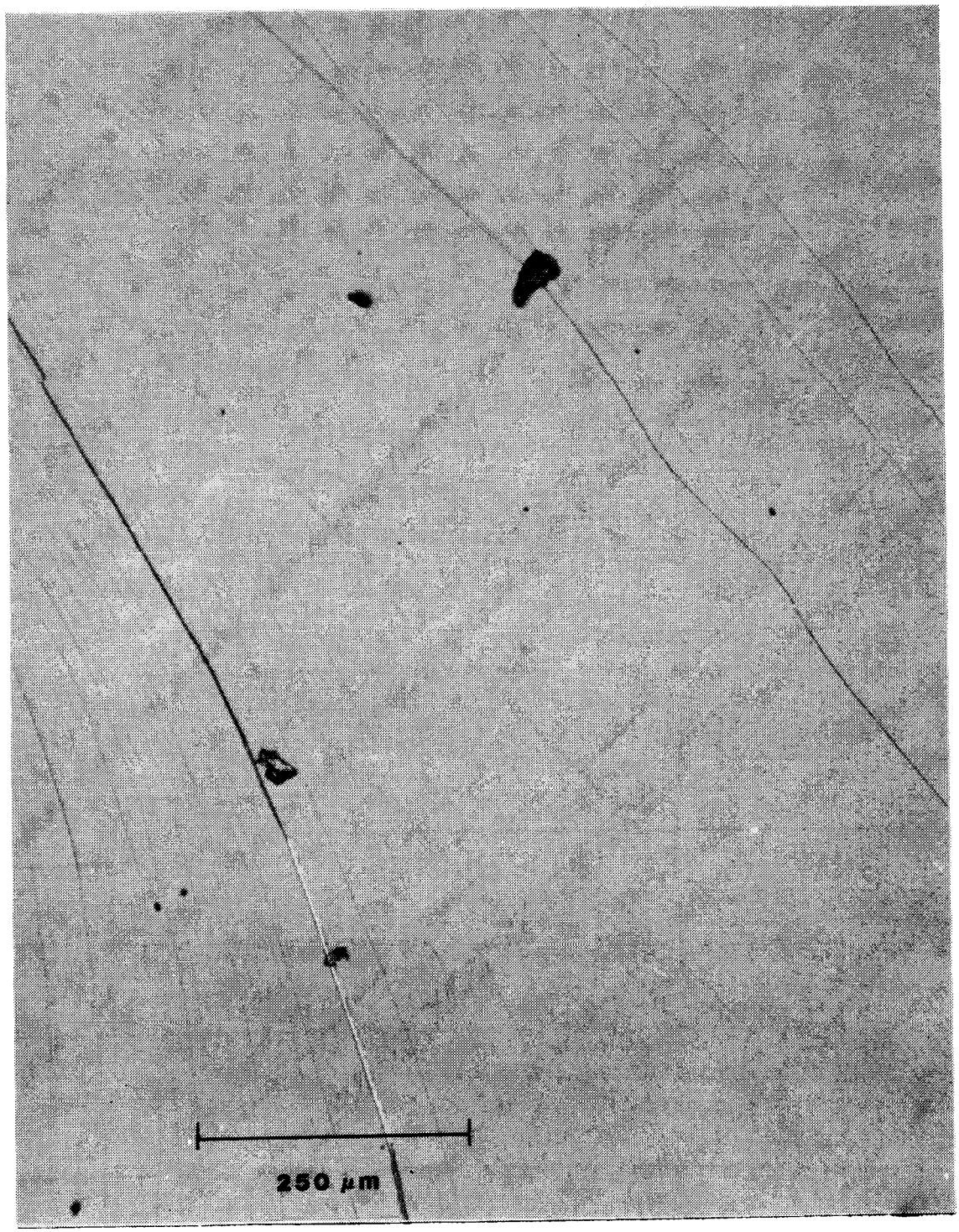

Figure 15a. Substructures in West Hackberry salt, sample WH108-2267 after laboratory testing (Table B2 and Figure C2).

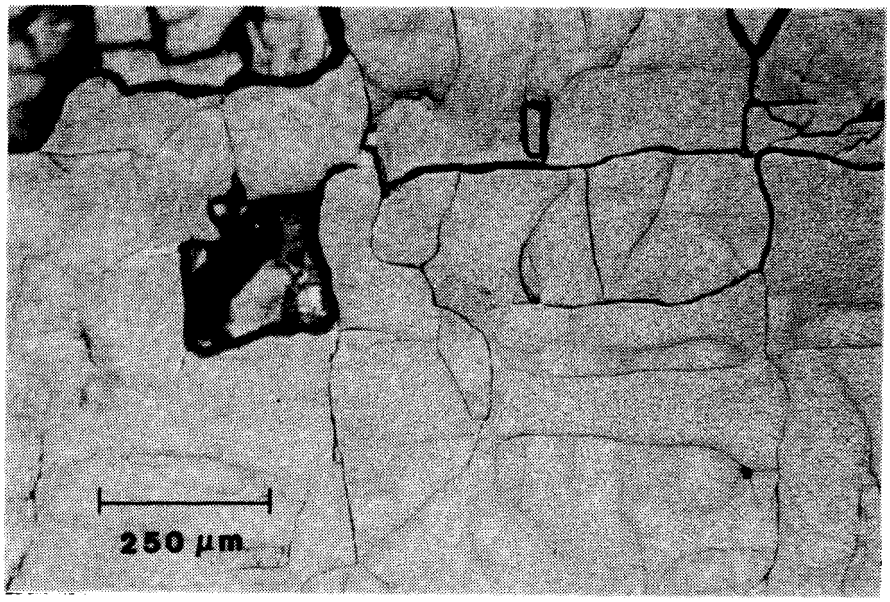

Figure 15b. Substructures in West Hackberry salt, sample WH108-2267 after laboratory testing (Table B2 and Figure **C2).**

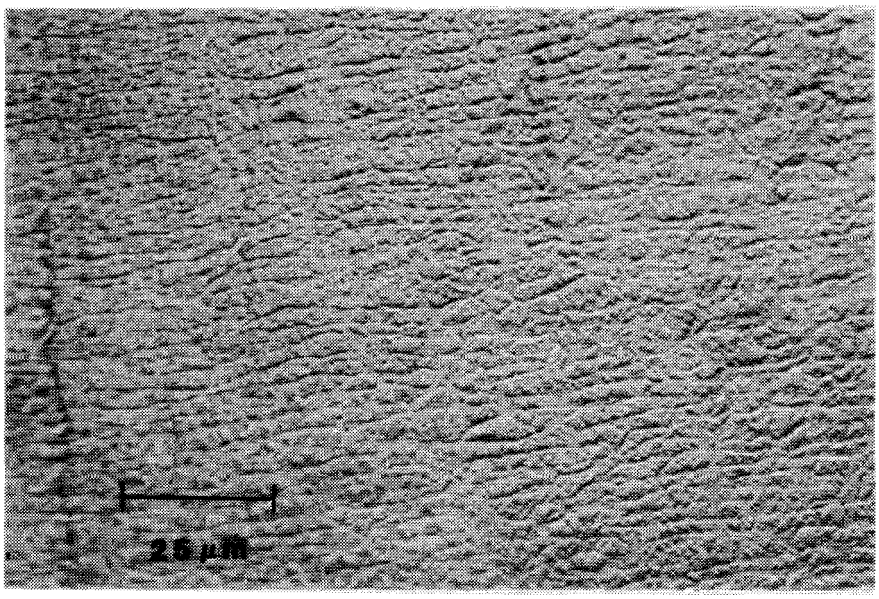

Figure 15c. Substructures in West Hackberry salt, sample WH108-2267 after laboratory testing (Table B2 and Figure C2).

Appendix A

Test matrices by site: West Hackberry, Bryan Mound, and Bayou Choctaw. Stresses are defined to within ± 25 psi. For details see Appendix B.

Table A1. Test Matrix for West Hackberry Salt

Nominal Stress, τ	Nominal Temperature °C	
psi	60	80
1970	X	
2030	0	0
2400		X
2440	⊗	
2770	0	
2925	×	
3010	○	

Legend by drillhole number and depth in ft (test I.D.):
× 108-3255 (QD12AN)
○ 108-3623 (QD11AN)

Table A2. Test Matrix for Bryan Mound Salt

Nominal Stress, τ psi	Nominal Temperature °C					
	22	33	40	60	80	100
2050				⊗	○	
2220				○	○	
2340				□		
2500			•	•	•	
2840			•	A	•	A
2980	A			0	0	
3220	+			⊛		
3270				□		
3550		0		0	0	

Legend by drillhole number (test I.D.) and depth (ft):

× 107C-2506 (QF34N)
○ 107C-2508 (QF35N)
\+ 107C-2516 (QF20N)
△ 108B-3324 (QF22AN)
□ 107C-2517 (QF36AN))
● 113-4225 (QF37N)

Table A3. Test Matrix for Bayou Choctaw Salt

Nominal Stress, σ psi	Nominal Temperature, °C	
	60	80
1860		×
2130	×	×
2470	×	

Appendix B

Results of creep measurements. $\dot{e}_{1b}$ is the creep rate at the beginning of each test stage. If stress was increased, then $\dot{e}_{1b}$ equals the secant slope to data recorded for 8 to **10** minutes beginning approximately 2 minutes after the stress change. Otherwise, $\dot{e}_{1b}$ as well as $\dot{e}_{1e}$, the creep rate towards the end of each stage, were obtained by means of linear least-squares fits to between 15 and 60 data points.

Test QF22AN (Table B4) was performed at 500 psi confining pressure, except for stage 2, which was carried out at 3000 psi confining pressure. The confining pressure in all other tests was 2000 psi. It is emphasized that the change in confining pressure in test QF22AN was effected at constant shear stress τ.

The stress values shown are true stresses: i.e., nominal stresses corrected for cross-sectional changes of the samples.

Table B1. Test Data

Origin of **Salt: West Hackberry WH108-3652.5**

Test I.D.	Stage No.	Time Incr.	τ	T	Strain Incr.	Strain Rate, $10^{-8}\ s^{-1}$	
		hrs	psi	°C	%	$\dot{e}_{1b}$	$\dot{e}_{1e}$
QD12AN	1	287	$1972\left(^{+57}_{-95}\right)$	60	2.07	210.9	0.88
	2	193	$2435\left(^{+107}_{-60}\right)$	60	2.71	164.1	2.48
	3	118	$2400\left(^{+143}_{-124}\right)$	80	2.42	9.06	6.59
	4	146	$2457\left(^{+49}_{-35}\right)$	60	1.21	0.83	1.63
	5	101	$2925\left(^{+88}_{-102}\right)$	60	3.30	>70.3	6.19
	6	167	$2424\left(^{+65}_{-60}\right)$	60	1.38	0.40	2.75

Table B2. Test Data

Origin of Salt: **West** Hackberry **WH108-2267**

Test I.D.	Stage No.	Time **Incr.** hrs	τ psi	T °C	Strain **Incr.** %	Strain Rate, $10^{-8}\ s^{-1}$ $\dot{e}_{1b}$	$\dot{e}_{1e}$
QD11AN	1	148	$3010\ (^{+58}_{-79})$	60	**9.48**	852.7	5.96
	2	104	$2722\ (^{+44}_{-29})$	60	0.38	0.54	1.30
	3	112	$2441\ (^{+37}_{-45})$	60	0.07	0.205	0.208
	4	163	$2034\ (^{+34}_{-43})$	60	0.004	0.003	0.003
	5	121	$2028\ (^{+24}_{-29})$	80	0.073	0.106	0.38

Table B3. Test Data

Origin of Salt: Bryan Mound (BM) 107C-2516

Test I.D.	Stage No.	Time Incr. hrs	τ psi	T °C	Strain Incr. %	Strain Rate, $10^{-8}\ s^{-1}$ $\dot{e}_{1b}$	$\dot{e}_{1e}$
QF20N	1	313	$3030\left(^{+68}_{-42}\right)$	22	1.80	296.4	0.212
	2	311	$3048\left(^{+96}_{-90}\right)$	60	0.66	1.08	0.559

Table B4. Test Data

Origin of Salt: Bryan Mound (BM) 108B-3324

Test I.D.	Stage No.	Time Incr. hrs	τ psi	T °C	Strain Incr. %	Strain Rate, 10^{-8} s^{-1} $\dot{\epsilon}_{1b}$	$\dot{\epsilon}_{1e}$
QF22AN	1	143	$2986\,(^{+28}_{-64})$	22	2.41	109.4	0.92
	2	67	$3051\,(^{+34}_{-29})$	22	0.45		0.41
	3	120	$2966\,(^{+53}_{-36})$	22	0.905		0.27
	4	118	$2884\,(^{+70}_{-31})$	60	0.59	2.37	0.87
	5	99	$2891\,(^{+46}_{-84})$	100	4.15	16.29	9.69
	6	101	$2913\,(^{+15}_{-25})$	60	0.08	0.44	0.49

Table BS. Test Data

Origin of Salt: Bryan Mound (BM) 107C-2506

Test I.D.	Stage No.	Time Incr.	τ	T	Strain Incr.	Strain Rate, $10^{-8}\ s^{-1}$	
		hrs	psi	°C	%	$\dot{\epsilon}_{1b}$	$\dot{\epsilon}_{1c}$
QF34AN	1	700	$2064\ (^{+124}_{-41})$	60.4	1.31	164.4.	0.16
	2	139	$3150\ (^{+128}_{-109})$	60.2	2.39	116.2	1.10

Table B6. Test Data

Origin of Salt: Bryan Mound (BM) 107C-2508

Test I.D.	Stage No.	Time Incr.	τ	T	Strain Incr.	Strain Rate, $10^{-8}\ s^{-1}$	
		hrs	psi	°C	%	$\dot{\varepsilon}_{1b}$	$\dot{\varepsilon}_{1e}$
QF35N	1	361	$2034\,(^{+25}_{-34})$	59.7	0.81	64.8	0.11
	2	74	$2037\,(^{+43}_{-53})$	79.8	0.10		0.26
	3	94	$2084\,(^{+15}_{-13})$	79.8	0.10		0.27
	4	148	$2083\,(^{+25}_{-12})$	59.8	0.04	0.185	0.06
	5	337	$2231\,(^{+30}_{-49})$	59.8	0.11	8.41	0.074
	6	258	$2215\,(^{+30}_{-49})$	80	0.24	0.56	0.24
	7	246	$2212\,(^{+27}_{-16})$	59.6	0.04	0.07	0.047
	8	356	$2983\,(^{+39}_{-36})$	59.5	1.28	73.10	0.43
	9	364	$2972\,(^{+38}_{-34})$	80	1.60	1.76	0.914
	10	307	$2977\,(^{+34}_{-20})$	59.4	0.24	0.204	0.22
	11	269	$3202\,(^{+29}_{-21})$	59.4	1.21	>27.8	0.328
	12	483	$3556\,(^{+25}_{-17})$	59.4	0.77	204.2	0.96
	13	137	$3546\,(^{+43}_{-51})$	80	2.01	4.71	3.65
	14	328	$3546\,(^{+34}_{-61})$	33.5	0.24	0.14	0.12-0.14

Table B7. Test Data

Origin of **Salt: Bryan Mound (BM) 107C-2517**

Test I.D.	Stage No.	Time Incr. hrs	τ psi	T °C	Strain Incr. %	Strain Rate, 10^{-8} s^{-1} $\dot{\varepsilon}_{1b}$	$\dot{\varepsilon}_{1e}$
QF36N	1a	74	$2325\left(^{+41}_{-32}\right)$	59	-	54.14	0.281
	1b	42	$2356\left(^{+11}_{-2}\right)$	59	1.26	-	0.278
	2	214	$3270\left(^{+5}_{-3}\right)$	59	1.67	331.1	0.669

Table B8. Test Data

Origin of Salt: Bryan Mound (BM) 113-4225

Test I.D.	Stage No.	Time Incr. hrs	τ psi	T °C	Strain Incr. %	Strain Rate, 10^{-8} s^{-1} $\dot{e}_{1b}$	$\dot{e}_{1e}$
QF37N	1	163	$2500\ (^{+21}_{-13})$	40	1.96	218.3	1.085
	2	144	$2496\ (^{+22}_{-13})$	60	1.64	4.31	2.32
	3	50	$2478\ (^{+29}_{-20})$	80	1.48	11.68	8.50
	4	97	$2488\ (^{+7}_{-8})$	59.8	0.47	1.45	1.28
	5	404	$2490\ (^{+24}_{-7})$	39.8	0.07	0.284	0.296
	6	147	$2848\ (^{+20}_{-10})$	40	0.65	85.5	0.853
	7	95	$2836\ (^{+26}_{-16})$	59.8	1.28	4.51	3.28
	8	193	$2842\ (^{+24}_{-7})$	40	0.40	0.597	0.563
	9	53	$2830\ (^{+33}_{-34})$	79.6	2.73	18.35	12.58
	10	114	$2844\ (^{+22}_{-16})$	59.8	1.09	2.119	3.316

Table B9. Test Data

Origin of Salt: Bayou Choctaw (BC) 19A-2577/2.0

Test I.D.	Stage No.	Time Incr. hrs	τ psi	T °C	Strain Incr. %	Strain Rate, 10^{-8} s^{-1} $\dot{\epsilon}_{1b}$	$\dot{\epsilon}_{1e}$
QG4N	1	480	$2129\left(^{+49}_{-113}\right)$	60	1.79	180.9	0.349
	2	313	$2135\left(^{+30}_{-11}\right)$	80	1.27	1.67	0.816
	3	44	$1857\left(^{+24}_{-17}\right)$	80	0.013	0.056	0.08
	4	268	$2138\left(^{+29}_{-14}\right)$	80	0.73	-	0.66
	5	66	$1834\left(^{+19}_{-12}\right)$	80	0.015	0.073	0.046
	6	175	$2133\left(^{+3}_{-12}\right)$	80	0.396	-	0.55
	7	305	$2139\left(^{+28}_{-15}\right)$	60	0.11	0.099	0.113
	8	2	$2475\left(^{+15}_{-27}\right)$	60	0.075	>23.4	-
	9	266	$2152\left(^{+21}_{-15}\right)$	60	0.064	0.058	0.068
	10	24	$2462\left(^{+21}_{-12}\right)$	60	0.14	27.78	0.37
	11	145	$2159\left(^{+27}_{-14}\right)$	60	0.024	(0.057)	0.047
	12	407	$2471\left(^{+34}_{-22}\right)$	60	0.736	18.51	0.37
	13	91	$2151\left(^{+11}_{-13}\right)$	60		0.03	0.01

Appendix C

Creep records corresponding to measurements in Tables B1-B9. The strain e_1 denotes greatest, natural compressive strain.

Circled offsets between test stages are caused by unedited, quasi-instantaneous length changes with changes in temperatures.

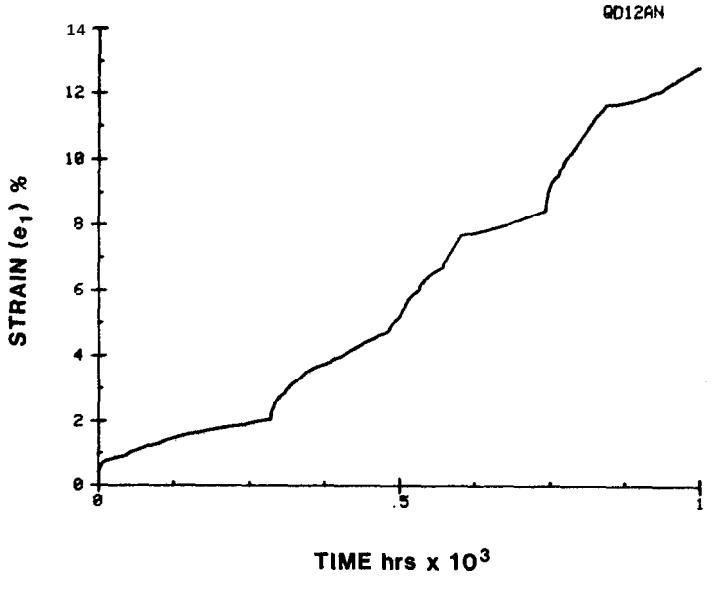

Figure C1. Creep curve for sample WH108-3652.5 (Table B1)

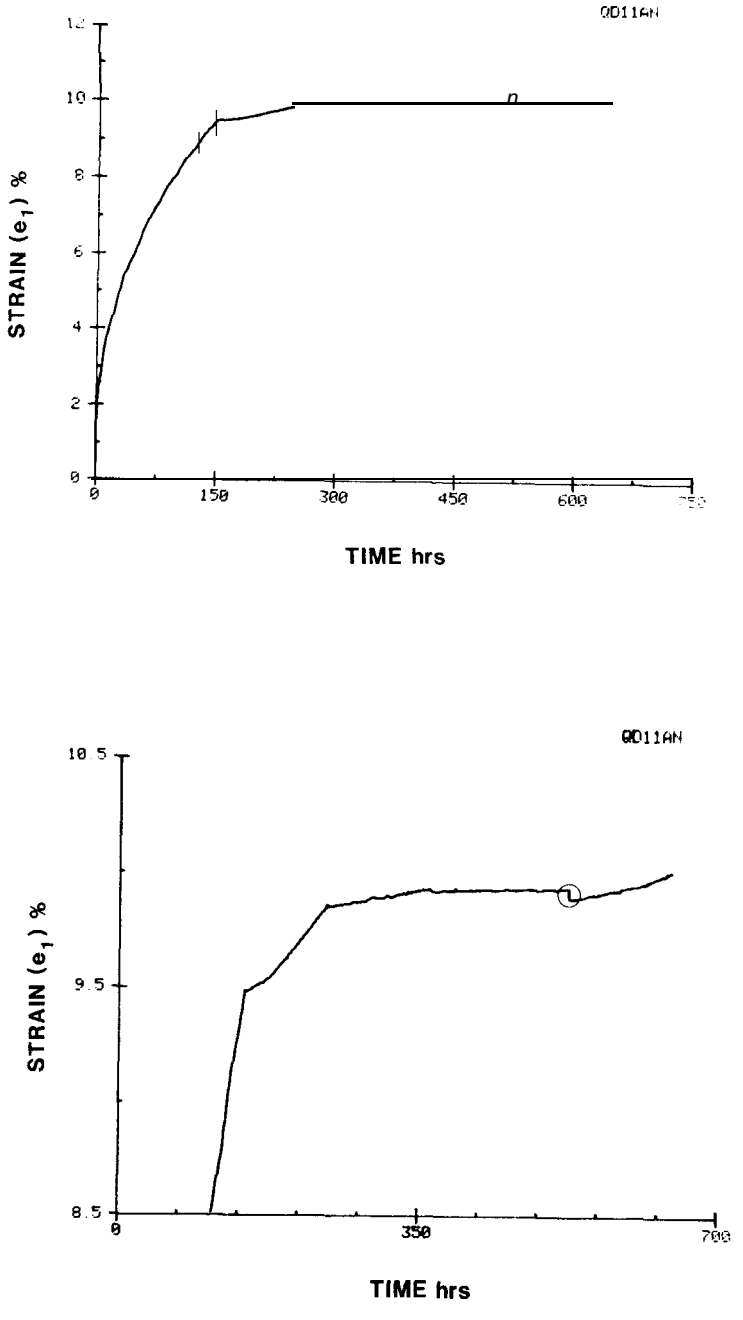

Figure C2. Creep curve for sample WH108-2267 (Table B2)

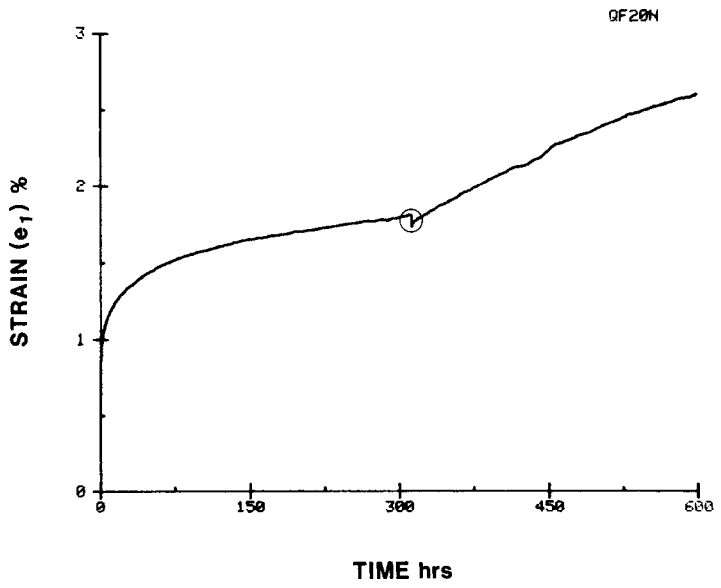

Figure C3. Creep curve for sample BM107C-2516 (Table B3)

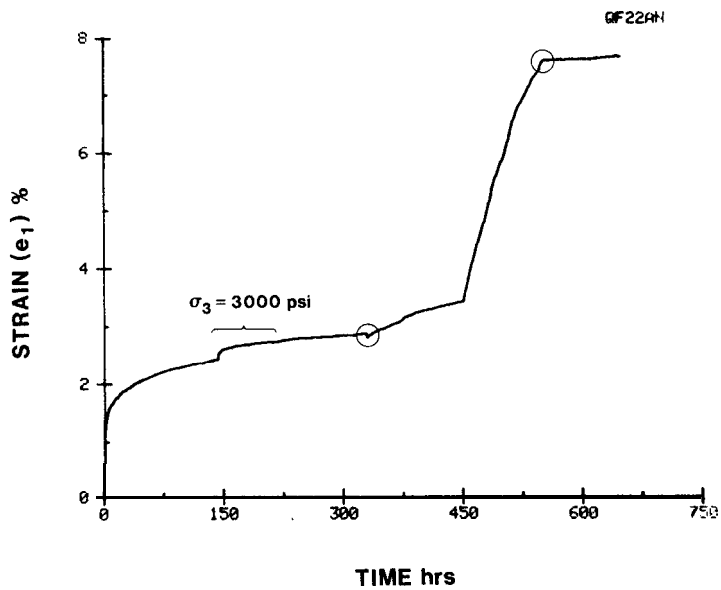

Figure C4. Creep curve for sample BM108B-3324 (Table B4)

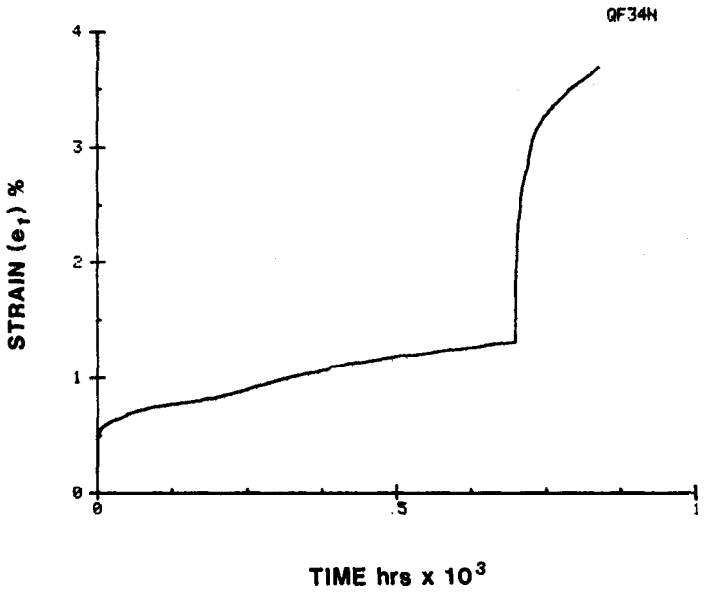

Figure CS. Creep curve for sample BM107C-2506 (Table B5)

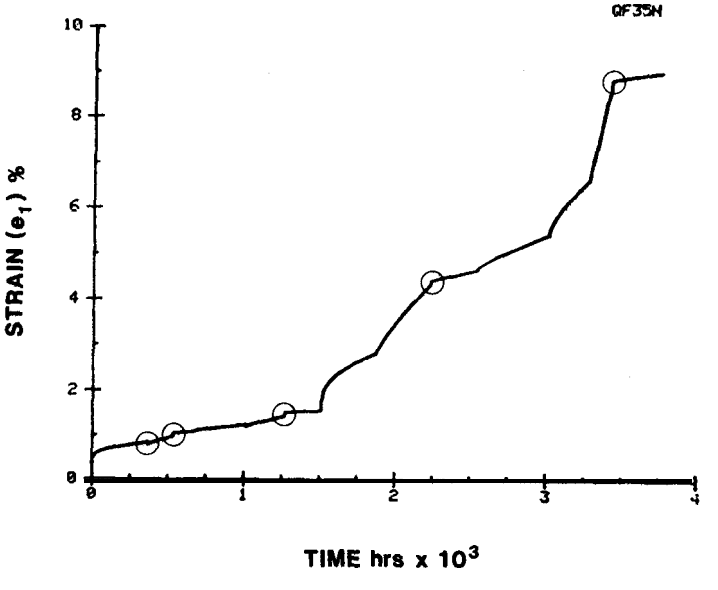

Figure C6. Creep curve for sample BM107C-2508 (Table B6)

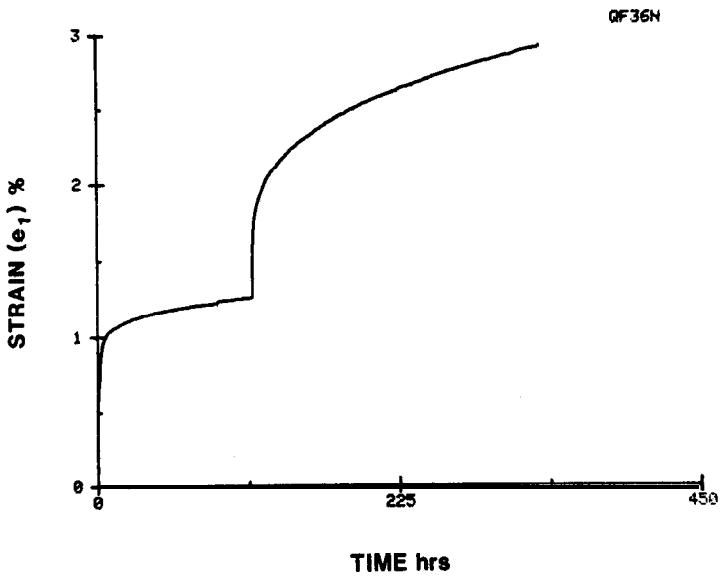

Figure C7. Creep curve for sample BM107C-2517 (Table B7)

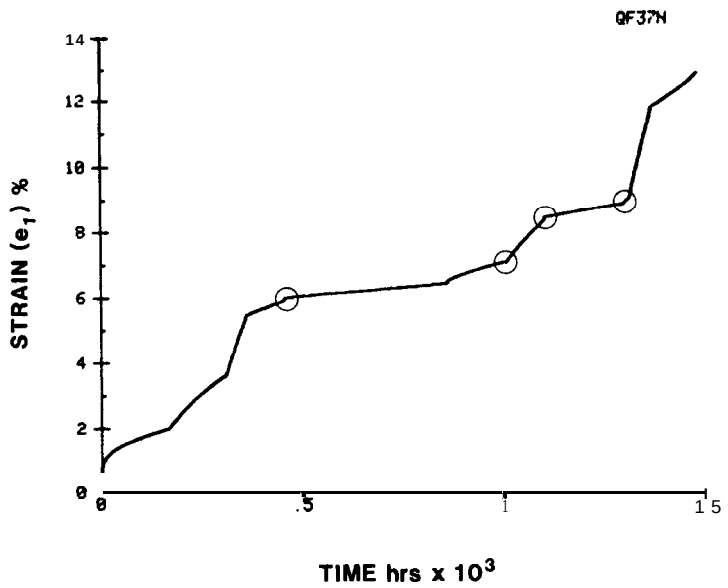

Figure C8. Creep curve for sample BM113-4225 (Table B8)

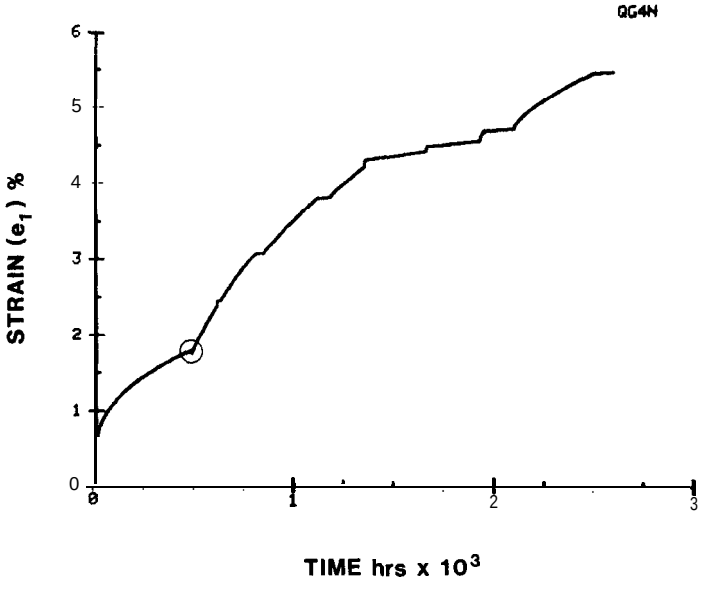

Figure C9. Creep curve for sample BM107C-2506 (Table B9)

Appendix D

Creep data for salt from the domes at West Hackberry and Bryan Mound that were presented in earlier reports, SAND79-0668 and SAND80-1434 [3,4].

Table D1. Test Data

Origin of Salt: West Hackberry

(Data from SAND740668)

Test I.D. (Sample I.D.)	Stage No.	Time Incr. hrs	Average Stress, τ psi	T °C	Strain Incr. %	Strain Rate, $10^{-8}\ s^{-1}$ $\dot{\epsilon}_{1b}$
CD8AN (6C-2243)	1	475	2960	22	3.58	0.95
CD9AN* (6C-2225)	1	263	2900	60	1.47	7.23
CD6AN (6C-2201)	1	262	2900	22	11.16	1.19
CD7AN* (6C-2196)	1	74	2890	60	4.52	5.97

* Triaxial extension test

Table D2. Test Data

Origin of Salt: Bryan Mound

(Data from SAND80-1434)

Test I.D. (Sample I.D.)	Stage No.	Time Incr. hrs	Average Stress, τ psi	T °C	Strain Incr. %	Strain Rate, 10^{-8} s^{-1} $\dot{\epsilon}_{1b}$
QF8N (107A-3966)	1	410	1470	60	0.48	0.252
QF9N (107A-2966)	2	332	3135	60	0.90	2.20
QF12N* (107A-3965)	1	457	3020	60	1.87	0.91
QF14N (107C-2507)	1	280	2990	22	1.51	2.75
QF16N (107C-2504.5)	1	264	2990	22	1.05	1.24

* Triaxial extension test

DISTRIBUTION: Category UC-92

U.S. Department of Energy, Headquarters
Office of Nuclear Waste Management
Washington, DC 20545
L. Harmon, Project Coordinator (WIPP)
W. W. Ballard
C. L. Cooley

U.S. Department of Energy, Albuquerque Operations
P. 0. Box 5400
Albuquerque, NM 87185
G. C. Romatowski
W. R. Cooper, WIPP Project Office (2)
D. G. Jackson, Director, Public Affairs Division

U.S. Department of Energy
Carlsbad WIPP Project Office
Room 113, Federal Building
Carlsbad, NM 88220

U.S. Department of Energy, NPO
Office of Nuclear Waste Isolation
505 King Avenue
Columbus, OH 43201
Jeff 0. Neff
Ram B. Lahoti

U.S. Nuclear Regulatory Commission
Division of Waste Management
Mail Stop 697SS
Washington, DC 20555
Michael Bell
Hubart Miller

Battelle Memorial Institute
Project Management Division
505 King Avenue
Columbus, OH 43201
N. E. Carter, General Manager (3)
S. Goldsmith
S. Basham
W. Carbiener
R. Heineman
P. Hoffman
J. Kircher
M. Lemcoe
S. Matthews
D. Moak
J. Moody
R. Nicks
G. Raines
A. Coyle
ONWI Library

Westinghouse Electric Corporation
P. 0. Box 40039
Albuquerque, NM 87196
G. Hohmann
R. Jones (TSC)
V. Likar

Bechtel Inc.
P. 0. Box 3965
45-11 -B34
San Francisco, CA 94119
E. Weber
D. Roberts
H. Taylor
P. Frobenius
c. L. wu
D. L. Wu
N. Antonas
W. T. Li
B. R. Chytrowski

National Academy of Sciences, WIPP Panel

Frank L. Parker, Chairman
Department of Environmental and Water Resources Engineering
Vanderbilt University
Nashville, TN 37235

Konrad B. Krauskopf, Vice Chairman
Department of Geology
Stanford University
Stanford, CA 94305

Dr. Karl P. Cohen, Member
928 N. California Avenue
Palo Alto, CA 94303

Neville G. W. Cook, Member
Dept. of Material Sciences and Engineering
University of California at Berkeley
Heart Mining Building, #320
Berkeley, CA 94720

Fred M. Ernsberger, Member
205 Old Mill Road
Pittsburgh, PA 15238

Dr. Harold James, Member
1617 Washington Street
Port Townsend, WA 98368

Richard R. Parizek, Member
Department of Hydrogeology
Pennsylvania State University
University Park, PA 16802

D'Arcy A. Shock, Member
233 Virginia
Ponca City, OK 74601

John W. Winchester, Member
Department of Oceanography
Florida State University
Tallahassee, FL 32306

National Academy of Sciences
Committee on Radioactive Waste Management
2101 Constitution Avenue, NW
Washington, DC 20418
John T. Holloway, Senior Staff Officer

Hobbs Public Library
509 N. Ship Street
Hobbs, NM 88248
Ms. Marcia Lewis, Librarian

New Mexico Tech
Martin Speere Memorial Library
Campus Street
Socorro, NM 87810

New Mexico State Library
P. 0. Box 1629
Santa Fe, NM 87503
Ms. Ingrid Vollenhofer

Zimmerman Library
University of New Mexico
Albuquerque, NM 87131
Zanier Vivian

WIPP Public Reading Room
Atomic Museum, Kirtland East AFB
Albuquerque, NM 87185
Ms. Gwynn Schreiner

WIPP Public Reading Room
Carlsbad Municipal Library
101 S. Hallagueno Street
Carlsbad, NM 88220
Lee Hubbard, Head Librarian

Thomas Brannigan Library
106 W. Hadley Street
Las Cruces, NM 88001
Don Dresp, Head Librarian

Roswell Public Library
301 N. Pennsylvania Avenue
Roswell, NM 88201
Ms. Nancy Langston

State of New Mexico
Environmental Evaluation Group
320 Marcy Street
P. 0. Box 968
Santa Fe, NM 87503
Robert H. Neill, Director (2)

NM Department of Energy & Minerals
P. 0. Box 2770
Santa Fe, NM 87501
Larry Kehoe, Secretary
Kasey LaPlante, Librarian

Institut fur Tieflagerung
Theodor-Heuss-Strasse 4
D-3300 Braunschweig
Federal Republic of Germany
K. Kuhn
N. Jockwer
H. Gies

Michael Langer
Bundesanstalt fur Geowissenschaften
und Rohstoffe
Postfach 510 153
3000 Hannover 51
Federal Republic of Germany

Klaus Eckart Maass
Hahn-Meitner-Institut fur Kernforschung
Glienicker Strasse 100
1000 Berlin 39
Federal Republic of Germany

Rolf-Peter Rand1
Bundesministerium fur Forschung und Technologie
Postfach 200 706
5300 Bonn 2
Federal Republic of Germany

Helmut Rothemeyer
Physikalisch-Technische Bundesanstalt
Bundesanstalt 100, 3300 Braunschweig
Federal Republic of Germany

Argonne National Laboratory
9700 South Cass Avenue
Argonne, IL 60439
S. Fried
A. M. Friedman
N. Meldgin
M. Steindler

Battelle Pacific Northwest Laboratories
Battelle Boulevard
Richland, WA 99352
D. J. Bradley
J. Relyea
R. P. Turcotte
R. E. Westerman

Brookhaven National Laboratory
Upton, NY 11973
P. Colombo, Dept. of Applied Sciences
Cal Brewster, Bldg. 830

F. R. Cook
HLW Licensing Branch, Materials Section
MS 905 SS
Nuclear Regulartory Commission
Washington, DC 20555

D'Appolonia Consulting Engineers, Inc.
10 Duff Road
Pittsburgh, PA 15235
R. Ellison

D'Appolonia Consulting Engineers, Inc.
2350 Alamo SE
Suite 103
Albuquerque, NM 87106
D. Stephanson
A. K. Kuhn
D. Shukla
R. McKinney

Dr. Paul R. Dawson
254 Upson Hall
Dept. Mech. & Aerospace Engr.
Cornell University
Ithaca, NY 14853

E. I. Dupont de Nemours Company
Savannah River Laboratory
Aiken, SC 29801
M. J. Plodinec
G. G. Wicks
D. Witt

Dr. D. K. Mukherjee
Ontario Hydro Research Lab
800 Kipling Avenue
Toronto, Ontario, Canada
MBZ 554

R. E. Gerton
U.S. Department of Energy
Richland Operatons Office
Nuclear Fuel Cycle & Production Division
P. 0. Box 500
Richland, WA 99352

C. S. Fore
Ecological Sciences Information Center
Oak Ridge National Laboratory - Bldg. 2001
P. 0. Box X
Oak Ridge, TN 37830

John Handin
Center of Tectonophysics
Texas A&M University
College Station, TX 77840

Christopher S. John
J. F. T. Agapito & Associates, Inc.
715 Horizon Drive, Suite 340
Grand Junction, CO 81501

Kernforschung Karlsruhe
Postfach 3640
7500 Karlsruhe
Federal Republic of Germany
R. Koster
Reinhard Kraemer

D. E. Large
U.S. Department of Energy
Research & Technical Support Division
P. 0. Box E
Oak Ridge, TN 37830

Paul W. Levy, Senior Scientist
Brookhaven National Laboratory
Associated Universities, Inc.
Upton, NY 11973

D. E. Maxwell
Science Applications, Inc.
2450 Washington Avenue, Suite 120
San Leandro, CA 94577

Los Alamos Scientific Laboratory
Los Alamos, NM 87545
B. Erdal, CNC-11

University of Minnesota
Dept of Energy and Materials Science
151 Amundson Hall
421 Washington Avenue SE
Minneapolis, MN 55455
R. Oriani

Oak Ridge National Laboratory
Box Y
Oak Ridge, TN 37830
R. E. Blanko
E. Bondietti
C. Clairborn
G. H. Jenks

The Pennsylvania State University
Materials Research Laboratory
University Park, PA 16802
Della Roy
Rustum Roy

George Pinder
Department of Civil Engineering
Princeton University
Princeton, NJ 08540

Dr. R. 0. Pohl
Department of Physics
Clark Hall
Cornell University
Ithaca, NY 14853

RE/SPEC, Inc.
P. 0. Box 725
Rapid City, SD 57701
Dr. P. Gnirk
W. C. McLain
L. Van Sambeek
T. Pfeifle
R. Stickney

RE/SPEC, Inc.
P. 0. Box 14984
Albuquerque, NM 87191
S. W. Key

Rockwell International
Rocky Flats Plant
Golden, CO 80401
W. S. Bennett
C. E. Wickland

Rockwell International
Atomics International Division
Rickwell Hanford Operations
P. 0. Box 800
Richland, WA 99352
M. J. Smith
W. W. Schultz

E. Roedder
United States Department of the Interior
959 National Center
Geological Survey
Reston, VA

Dr. Shosei Serata
Serata Geomechanics
1229 Eighth Street
Berkeley, CA 94170

Svensk Karnbransleforsorjning AB
Project KBS
Karnbranslesakerhet
Box 5864
10248 Stockholm, SWEDEN
Fred Karlsson

Systems, Science, and Software
Box 1620
La Jolla, CA 92038
P. Lagus
E. Peterson

Titanium Metals Corp. of American
Henderson Technical Laboratory
P. 0. Box 2128
Henderson, NV 89015
R. W. Schutz

U.S. Army Engineers
Waterways Experiment Station
P. 0. Box 631
Vicksburg, MS 39180
J. Boa
K. Mather

U.S. Department of Energy
Division of Waste Products
Mail Stop B-107
Washington, DC 20545
G. H. Daly
J. E. Dieckhoner

U.S. Department of Energy
Idaho Operations Office
Nuclear Fuel Cycle Division
550 Second Street
Idaho Falls, ID 83401
R. M. Nelson
J. Whitsett

U.S. Department of Energy
Savannah River Operations Office
Waste Management Project Office
P. 0. Box A
Aiken, SC 29801
J. R. Covell
D. Fulmer

U.S. Geological Survey
Special Projects
MS954, Box 25046
Denver Federal Center
Denver, CO 80255
R. Synder

U.S. Geological Survey
P. 0. Box 26659
Albuquerque, NM 87125
J. Mercer

University of Arizona
Department of Nuclear Engineering
Tucson, AZ 85721
J. G. McCray
J. J. K. Daemen

University of New Mexico
Geology Department
Albuquerque, NM 87131
D. G. Brookins

Woodward-Clyde Consultants
Library Western Region
3 Embarcadero Center, Suite 700
San Francisco, CA 94111
Anne T. Harrigan, Librarian
Charles Taylor

U.S. DOE SPR PMO
900 Commerce Road East
New Orleans, LA 70123
E. E. Chapple, PMO-581 (6)
L. Smith, TDCS (2)

U.S. Department of Energy
Strategic Petroleum Reserve
1000 Independence Avenue SW
Washington, DC 20585
Dave Johnson
Dick Smith

U.S. Department of Energy
Oak Ridge Operations Office
P. 0. Box E
Oak Ridge, TN 37831
P. Brewington, Jr.

Aerospace Corporation
800 Commerce Road East, Suite 300
New Orleans, LA 70123
K. Henrie
R. Merkle

Walk-Haydel & Associates
600 Carondelet
New Orleans, LA 70112
R. Haney

POSSI
850 S. Clearview Parkway
New Orleans, LA 70123
K. Mills

Dr. H.-J. Bathe
Department of Civil Engineering
Massachussetts Institute of Technology
Cambridge, MA 02139

Dr. W. F. Brace, Chairman
Department of Earth, Atmospheric, and Planetary Scienc
Room 54-918
Massachussetts Institute of Technology
Cambridge, MA 02139

Bundesansalt fuer Geowissenschaften und Rohstoffe
Postfach 51 01 53
3000 Hannover 51
Federal Republic of Germany
Dr. U. Hunsche
Dr. M. Wallner

Dr. N. L. Carter
Center for Tectonophysics
Texas A&M University
College Station, TX 77843

Dr. P. Dawson
Department of Mechanical and Aerospace Engineering
254 Upson Hall
Cornell University
Ithaca, NY 14853

Dr. C. Fairhurst
Department of Civil and Mineral Engineering
University of Minnesota
Minneapolis, NM 55455

Dr. R. H. Hardy, Jr.
Department of Mineral Engineering
The Pennsylvania University
104 Mineral Science Building
University Park, PA 16802

Dr. H. C. Heard
Mail Stop L201
Earth Science Department
University of California
Lawrence Livermore National Laboratory
P. 0. Box 808
Livermore, CA 94550

Dr. B. Ladanyi
Department of Mineral Engineering
Ecole Polytechnique
2500, Avenue Marie-&yard
Montreal 250
Canada

Dr. K.-H Lux
Institut fuer Unterirdisches Bauen
Universitaet Hannover
3000 Hannover 1
Welfengarten 1
Federal Republic of Germany

Dr. A. Mahtab
Henry Krumb School of Mines
Columbia University
New York, NY 10027

Dr. G. M. Pharr
Dept. of Mechanical Engineering and Material Science
Rice University
P. 0. Box 1892
Houston, TX 77251

Dipl.-Ing. G. Staupendahl
Institut fuer Tieflagerung
Theodor-Heuss-Strasse4
3300 Braunschweig
Federal Republic of Germany

RE/SPEC, Inc.
P. 0. Box 725
Rapid City, SD 57701
Dr. P. Senseny
Dr. F. D. Hansen

Dr. R. L. Thorns
Applied Geomechanics, Inc.
P. 0. Box 80619
Baton Rouge, LA 70898

0311 D. R. Fortney
0311 H. C. Shefelbine
1510 J. W. Nunziato
1511 G. C. Weigand
1511 G. R. Hadley
1512 J. C. Cummings
1520 D. J. McCloskey
1521 R. D. Kreig
1521 H. S. Morgan
1521 D. S. Preece
1521 C. M. Stone
1524 L. J. Branstetter
1530 L. W. Davison
1531 B. J. Thorne
1540 W. C. Luth
1542 B. M. Butcher
1542 D. W. Hannum
1542 M. F. Shields
1542 L. W. Teufel
1542 W. R. Wawersik (20)
1542 D. H. Zeuch (10)
1543 J. L. Krumhansl
1800 R. L. Schwoebel
1812 L. A Harrah
1820 R. E. Whan
1821 N. E. Brown
1821 R. W. Bild
1822 K. H. Eckelmeyer
1824 J. N. Sweet
1824 M. Moss
1830 M. J. Davis
1832 W. B. Jones
1840 R. J. Eagan
1841 W. L. Larson
1841 R. S. Glass
1843 C. J. M. Northrup, Jr.
1843 R. G. Dosch
1843 E. J. Nowak
3310 W. D. Burnett
6000 E. H. Beckner
6200 V. L. Dugan
6250 B. W. Marshall
6253 D. A. Northrop
6253 A.R. Sattler
6257 J. K. Linn (10)
6257 R. R. Beasley
6257 S. T. Wallace
6257 K. L. Goin
6300 R. W. Lynch
6310 T. 0. Hunter

6311 L. W. Scully
6311 P. D. O'Brien
6312 F. W. Bingham
6312 J. K. Johnston
6313 J. R. Tillerson
6330 W. D. Weart
6330 J. T. Henderson
6331 A. R. Lappin
6331 G. E. Barr
6331 D. D. Gonzalez
6331 S. J. Lambert
6331 W. B. Miller
6331 K. L. Robinson
6331 S. E. Shaffer
6332 L. D. Tyler (10)
6332 C. L. Christensen
6332 D. M. Ellett
6332 R. V. Matalucci (5)
6332 M. A. Molecke
6332 D. E. Munson
6332 J. C. Stormont
6332 T. M. Torres
6332 Sandia WIPP Central Files (HLW) (2)
6333 M. L. Merritt
6334 L. H. Brush
7000 R. L. Peurifoy
7100 C. D. Broyles
7110 J. D. Plimpton
7112 C. R. Mehl
7112 G. H. Miller
7116 S. R. Dolce
7116 E. S. Ames
7116 C. W. Cook
7120 T. L. Pace
7125 G. L. Ogle
7125 J. T. McIlmoyle
7130 J. D. Kennedy
7133 R. D. Statler
7133 C. W. Gulick, Jr.
7135 P. D. Seward
7500 E. E. Ives
7550 F. W. Neilson
7554 G. L. Maxam
7554 R. I. Ewing
8120 L. D. Bertholf
8314 S. L. Robinson
8314 N. R. Moody
8314 M. W. Perra
8315 L. A. West
8315 D. H. Doughty

8424 M. A. Pound
3141 C. Ostrander (5)
3144 W. R. Roose (5)
3151 W. L. Garner (3)
3154-3 C. H. Dalin (25) DOE/TIC (Unlimited Release)